Lateral Migration of Particles Under Poiseuille Flow

Rafil Fikriyan

Technische Universiteit Delft

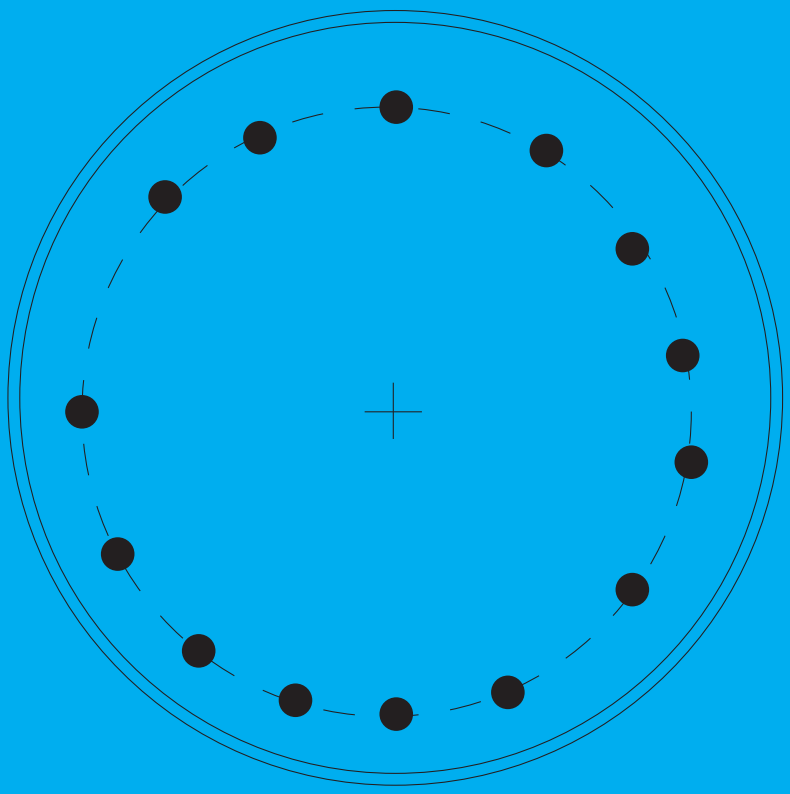

TU Delft

Lateral Migration of Particles Under Poiseuille Flow

by

Rafil Fikriyan

to obtain the degree of Master of Science
at the Delft University of Technology,
to be defended publicly on Thursday March 28, 2019 at 15:00 PM.

Student number:	4613198	
P&E report number:	2963	
Thesis committee:	Prof. dr. ir. C. Poelma,	TU Delft, Supervisor
	Dr. ir. B. Eral,	TU Delft
	Ir. W. Hogendoorn,	TU Delft, Daily Supervisor

TU Delft

Preface

This master thesis is a proof that everything is possible in this life. I have to be honest that this moment is one of the most challenging time so far in my life. Nevertheless, this is a precious experience that has improved me as a person.

First of all, praise be to Allah SWT, Most Gracious, so that I can finish my study.

I would like to thank my supervisor, Prof. Christian Poelma for the opportunity to work on this thesis project. Before doing this thesis I never have the experience to conduct a proper experiment in the multiphase field, with his expertise and guidance now I can finish this thesis study.

During this thesis study, I have two great daily supervisors. Firstly, Cenk Cetin who has guided me at the early time of working my thesis. Secondly, Willian Hoogendorn who spared his time to guide me in finishing my thesis report. Both of you accepted me not only as a student who wanted to finish his work but also as a friend during my time in the laboratorium.

Dr. Burak Eral as my committee member I would like to thank you for your willingness to become a committee for my thesis defense. I remember you from Equipment of Heat & Mass transfer course. You always teach with full of energy which brings enthusiasm for the students who attended the class.

Thank you for my family, especially both of my parents who relentlessly pray for me and make sure that I am alright and be strong in the process of finishing the thesis. I would like to thank you all my TU Delft friends who become the place to share laugh and story during my study. Last, I would like to give a big love to Putri Suciaty Gandina who always become the mood booster through many ups and downs during my time here.

Rafil Fikriyan
Delft, March 2019

Abstract

Lateral migration of particles is the phenomenon in suspension flow which causes non-uniform distribution of the dispersed phase due to lateral movement of particles in unidirectional flow. Since its discovery, this phenomenon has brought a curiosity in the fluid mechanics field because it has been widely understood that in unidirectional flow there is only axial velocity component. Numerous studies have reported that the migration is due to the exerted force from the fluid to the particle. The migration is complete when the particle has reached the equilibrium position which has widely reported to be at the region between the tube-axis and tube-wall in a Poiseuille flow.

In this thesis the combined effect of flow Reynolds number and particle concentration on the particle migration in a Poiseuille flow is studied experimentally. Neutrally buoyant spheres with diameter d are used in the experiment as a dispersed phase. These two parameters have been reported to have opposing effects on the migration. An increase in Reynolds number brings the particle to migrate closer to the wall, while an increase in particle concentration generates a resistance to the movement of particles into the equilibrium position. To investigate this effect, Reynolds number is varied in the range $Re = 200 - 1200$ and particle concentration in the range $\phi = 0.05 - 0.5\%$. Particles radial positions are captured using particle tracking method for each combination of experimental parameter at multiple observation distances from the inlet.

The results reveal that the increase in Reynolds number leads to particles migrate at a longer distance to reach the equilibrium position. There is a decrease in the rate of particles accumulation at the equilibrium position with higher Reynolds number. With an increase in the particle concentration, it is shown that the probability to find the particles at the equilibrium position is decreasing. Moreover, the experiment result reveals that the effect of Reynolds number on the migration distance is less significant at higher particle concentration. The secondary phenomena following the particle migration, emergence of inner annulus and the formation of particle trains are also studied in this thesis study. It is shown that these secondary phenomena are highly related to the particles accumulation in the equilibrium position. Both phenomena are also observed to be affected by the variation in Reynolds number and particle concentrations.

Contents

List of Figures

List of Tables

Nomenclature

$\bar{\sigma}$	standard error
$\bar{r}_j$	particles positions in cylindrical coordinate
$\bar{x}_j$	particles position in cartesian coordinate
λ	wavelength of light
μ	dynamic viscosity
ϕ	% particle concentration
ρ	fluid density
ρ_p	particle density
$\vec{\Omega}$	particle angular velocity
$\vec{F}_{body}$	Body Force
$\vec{U}$	particle velocity
B	buoyancy number
D	tube diameter
d	particle Diameter
d_{sp}	average spacing between particle
d_s	diffraction limited diameter
d_t	diameter of particle image
f	frame rate of camera
$F\#$	camera apperture
F_f	total force exerted by the fluid to the particles
h	height of water surface to the reference height
L	distance from tube inlet
l	length of field of view
L_D	entrance length
M	magnification Factor
m_{part}	mass of the dispersed phase
m_p	mass of a particle
m_{sus}	mass of the suspensions
n	number of particles
n_{true}	true number of particles

p	pressure
$P(r/R)$	probability of particle at radial position r
P_{out}	probability of particle around the equilibrium position
R	tube radius
r	particle radius
Re	channel Reynolds number
Re_p	particle Reynolds number
$t_{r/R}$	number of frames of particles leaving the field of view
u_{max}	maximum axial velocity
U_m	particle mean axial velocity
u_s	settling velocity
V_{FoV}	volume of field of view
$V_{particle}$	volume of particle
Var	Variance of the measurement result
Z_0	distance of camera from the object
u_r	axial velocity at radial position r/R

1

Introduction

A suspension is a heterogeneous mixture of solid particles and a liquid, which can be classified as multiphase flows. The suspension has a wide range of applications in industry. Some examples are mudflows in the drilling process, sanitation management in the metropolitan areas, removal of sediment in the dredging process, and products distribution in pharmaceutical and cosmetic industries. These examples bring great interest to put an effort to understand the nature of a suspension, especially for the application of suspension flow. In recent days the physics behind suspension flow is still not well understood due to its inherent complexity. This condition results in inefficient design, low energy efficiency, and a conservative operational condition limit. The discovery of new tools and knowledge to study suspension has brought an observation to new underlying phenomena in suspension flows. To understand the physics behind the suspension flow, it is necessary to understand the behaviour of these phenomena.

When a suspension flows through a circular tube, the solid particles are not uniformly distributed over the cross-section of the tube. This phenomenon was first reported by Fahraeus and Lindqvist in 1931 [7]. They observed that the erythrocytes were concentrated at the tube axis during the blood flow experiment through a narrow capillary as seen in Figure 1.1. This non-uniformity has been understood due to the fluid exerts an axially directed transverse force on the particles. Based on this observation, it has been predicted that the particles under a shear flow will experience a lateral migration. This discovery has generated interest in the fluid mechanics field because previously it has widely understood that in the laminar unidirectional flow there is no other velocity component except in the axial direction. The radial motion of particles in unidirectional flow during the migration has brought curiosity to study the physics behind this phenomenon.

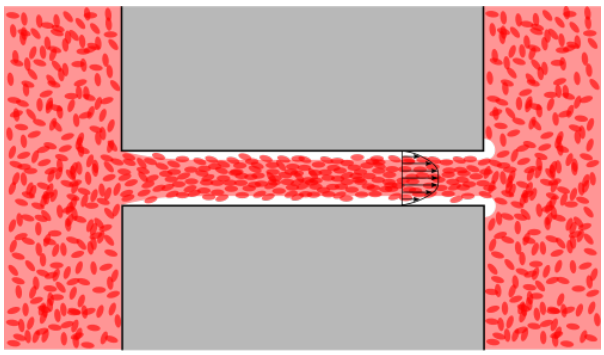

Figure 1.1: The accumulation of erythrocytes in the axis of the tube in Fahraeus and Lindqvist experiment. Figure Adapted from Wikipedia.org

A remarkable observation in the study of particle migration was reported by Segré and Silberberg in 1962 [38].They observed that when a dilute suspension of rigid spherical particles flowed through a circular tube in laminar flow, the particles would concentrate at the radial position about the halfway between the tube axis and tube walls (0.6 of the tube radii). The particles will continue to stay at this radial position, thus the radial position is also called as the equilibrium position. This phenomenon is called as the *Tubular Pinch Effect*, it is illustrated in Figure 1.2. The concentration of particles at the equilibrium position is forming an annular which is called as the Segré-Silberberg annulus.

The studies following the discovery of tubular pinch effect have reported the significance of flow Reynolds number in affecting the particle migration. Bretherton [4] shows through theoretical analysis that in a creeping flow, where the Reynolds number is very low, there is no migration occurred. This result was confirmed experimentally by Goldsmith and Mason [9]. With an increase in Reynolds number, the migration starts to occur, and the location of equilibrium position is progressively shifted closer to the wall [1, 22, 37]. What is not yet understood is the effect of Reynolds number to the migration-development distance, the distance of the particles reaching the equilibrium position from the inlet. Matas et al.[22] reported that the migration-distance is increasing with an increase in Reynolds number. While experimental evidence from Morita et al. [25] shows that the migration-distance increases with Reynolds number. This contradiction has brought a need to provide evidence to conclude the effect of Reynolds number to the development of particle migration.

Apart from the Reynolds number, particle migration is also affected by the particle concentration of the suspension. Previous studies have reported that an increase in particle concentration can create a condition where the particle-particle interaction becomes more frequent [10, 11, 18]. This interaction will suppress the migration of the particles into the equilibrium position and the particles are concentrated at the tube axis instead of the equilibrium position. Although studies have recognized the effect of particle concentration, most are restricted to the study at low Reynolds number. There is still uncertainty about the combined effect of Reynolds number and particle concentration to particle migration. This study is interesting because these parameters have a different effect to the migration, as mentioned before an increase in Reynolds number brings the particles away from the tube axis while an increase in particle concentration resists the particle to the tube axis.

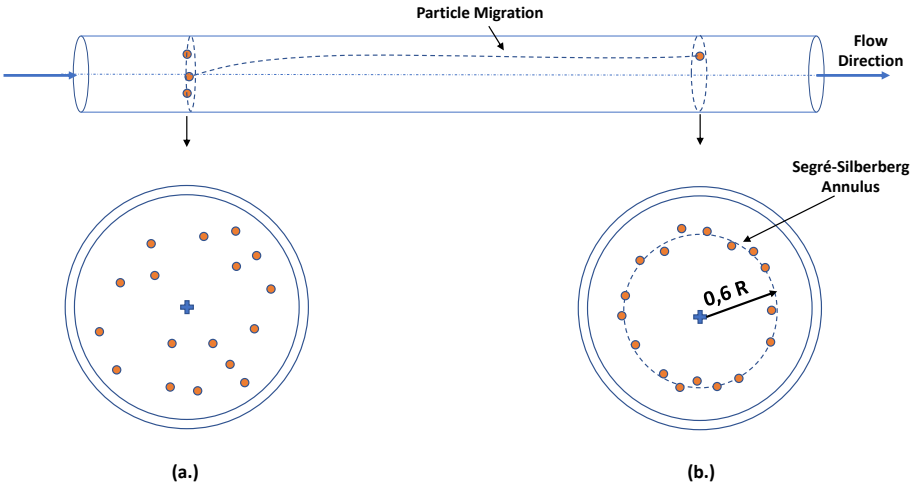

Figure 1.2: The illustration of Tubular Pinch Effect, (a.) Initially particles are uniformly distributed near the entrance, (b.) Particles experience a migration to reach the equilibrium position at 0.6 of tube radius to form the Segré-Silberberg Annulus.

In addition to the tubular pinch effect, it has been reported the occurrence of two secondary phenomena following the particle migration. Firstly, the generation of the second

annulus, beside Segré-Silberberg annulus, at flow Reynolds number above 600 which lies at the radial position close to the axis of the tube. This phenomenon was first observed by Matas et al.[22] in 2004, and they call the formed annulus as the inner-annulus. Secondly, the hydrodynamic interaction between particles leads to the formation of particle trains [21]. The particle trains are seen as the alignment of several particles in the direction of the flow to form a train like structure. These secondary phenomena are both presented in Figure 1.3. So far, however, there has been little discussion about these secondary phenomena. As a result, it remains unclear the nature of this secondary phenomena to the change in the flow parameter. Determining the effect of flow parameter to the secondary phenomena is essential for understanding the nature of suspension in general.

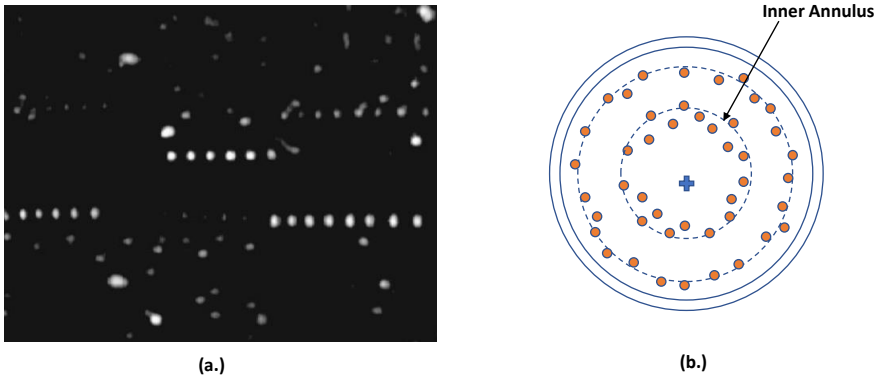

Figure 1.3: The secondary phenomena following the particle migration under laminar Poiseuille flow, (a.)Trains of particles, Figure reproduced from Matas et al. [21] and (b.)The illustration of the Inner Annulus.

This thesis will focus to study the effect of two parameters, Reynolds number and particle concentration, to the particle migration. From the literature study, there is a gap in understanding the combined effect of varying Reynolds number and particle concentration on the development of the particle migration into the equilibrium position. Furthermore, the occurrence of the secondary phenomena is still not well understood and need more explanation. The effect of varying these parameters on the mentioned secondary phenomena is an interesting subject in the effort to gain understanding about their natural behaviour. The study in this thesis project will rely on the particle tracking method which has a limitation in the concentration level of particles in the suspension. Early understanding of the effect of particle concentration and Reynolds number at low concentration is a small step towards the solid and complete understanding of the nature of the suspension flow.

1.1. Research Question

This study aims to enhance the physical understanding of the particle migration phenomena. The study will concentrate on the combination of the effect of particle concentration and Reynolds number into the development of the particles migration. There has been numerous study indicate the importance of these parameters in altering the occurrence of the phenomena. The research question can be formulated as:

"What is the effect of particles concentration and Reynolds number on the development of lateral migration of particles under Poiseuille flow?"

The main research question can be divided into several sub-questions:

1. How are the particles distributed at different particle concentrations and Reynolds num-

bers?

2. What is the effect of particle concentrations and Reynolds numbers into the occurrence of the secondary phenomena:

- How does the inner annulus develop at different particles concentration and Reynolds number?
- How do the trains of particle develop at different particle concentrations and Reynolds number along with the tube length?

In order to answer these questions, experiments are conducted to capture the radial position distribution of the particles in a Poiseuille flow. Radial position distribution is presented in the form of probability distribution at different Reynolds number, particle concentration, and observation distance.

1.2. Outline

This report starts with a theoretical background and literature review behind the phenomenon of particle migration in chapter 2. Chapter 3 presents the experimental set-up which is used in this thesis project. In chapter 4, several data processing steps, such as particle detection, 3D coordinate construction, and statistical correction are explained in a separate section. In chapter 5, the experimental results are presented, and the discussion is conducted to the physical phenomena that appears following the particle migration. The conclusion from the thesis project and recommendations for the future work finally are given in chapter 6.

2

Literature Study and Theoretical Background

This chapter discusses the theoretical background and previous studies in the subject of lateral migration of particles. Section 2.1 presents the physical background of the migration; it is divided into the presentation of the relevant parameters to the particle migration and the governing equation which is commonly used to analyze the fluid mechanic's case. The chapter continues with a brief introduction to the concept of lateral particle migration in section 2.2. Some of recent research and efforts to understand the importance of the inertial effect and the effect of particle concentration in suspension to the migration is presented in section 2.3. The chapter ended with important remarks from the literature study which relevant to the thesis study in section 2.4.

2.1. Physical Background

2.1.1. Relevant Parameters

A number of parameters are defined in the form of dimensionless number that are of importance for the particle migration. The importance of these parameters to particle migration have been reported by several studies, which will be discussed in detail in the next section.

Reynolds number is the ratio between the inertial force and the viscous force. Reynolds number is an important parameter in fluid mechanics as an indicator of which force is dominant in the flow. Reynolds number of the fluid flow is given by:

$$Re = \frac{\rho U_m D}{\mu} \tag{2.1}$$

Where ρ is the density of the fluid, U_m is the mean axial velocity of the flow which acts as the characteristic velocity scale of the fluid, D is the diameter of the tube which acts as the characteristic length scale, and μ is the viscosity of the fluid. At low Reynolds numbers, the viscous force is dominating the flow, and the flow regime is laminar. At High Reynolds numbers the inertial forces dominate the flows; this is the case when the flow is turbulence. The transitional Reynolds number from laminar to turbulence for pipe flow is at $Re = 2100$ [44].

When studying particle migration, it is also important to define the Particle Reynolds number (Re_p) to characterize the flow regime around particles. In which particle diameter (d) acts as the characteristic length. Re_p is defined as:

$$Re_p = \frac{\rho U_m d}{\mu} \tag{2.2}$$

Apart from the Reynolds number, when studying suspension flow, particle concentration (ϕ) is an important parameter to describe the dynamic condition between the particles. Particle concentration can be described as the ratio of the mass of the dispersed phase (m_{part}) over the mass of the flowing suspensions (m_{sus}) :

$$\phi = \frac{m_{part}}{m_{sus}} \times 100\% \tag{2.3}$$

From particle concentration, average particle spacing (d_{sp}) can be estimated using equation 2.4 from Poelma [30]:

$$d_{sp} = d\left(\frac{\pi}{6\phi}\right)^{1/3} \tag{2.4}$$

The flow geometry can be characterized by the ratio of particle axial distance from the inlet and tube diameter (L/D) and the ratio of particle diameter and tube diameter (d/D). The relevant parameter is summarized in table 2.1.

Table 2.1: Relevant parameters in the study of particle migration

Re	Bulk Reynolds number
Re_p	Particle Reynolds number
ϕ	Particle concentration in suspension
d_{sp}	Average particle spacing
L/D	ratio of axial distance of the particles from inlet and tube diameter
d/D	ratio of particle diameter and tube diameter

2.1.2. Governing Equation

Particle migration happens due to exerted force from the fluid to the particle. Therefore, in order to study the particle motion, it is usual to start by studying the flow field when there is a particle present. The flow field is governed by the laws of conservation of mass, momentum, and energy. Conservation of energy is neglected in this thesis study because it is assumed that the fluid has constant density (incompressible) and the temperature of the fluid is constant.

Conservation of mass of an incompressible Newtonian fluid is given by [2]:

$$\nabla \cdot \vec{u} = 0 \tag{2.5}$$

As for the conservation of momentum for an incompressible Newtonian fluid, is given by [2]:

$$\underbrace{\rho\frac{D\vec{u}}{Dt}}_{\textbf{Inertia}} = \underbrace{-\nabla p}_{\textbf{Pressure}} + \underbrace{\mu\nabla^2\vec{u}}_{\textbf{Diffusion}} + \underbrace{\sum \vec{F}_{body}}_{\textbf{Body Force}} \tag{2.6}$$

In equation 2.6, $\vec{u}$ is the velocity of the fluid, ρ is the density of the fluid, p is the pressure, and μ is the viscosity of the fluid. Equation 2.6 can be classified into four terms: inertia, pressure, diffusion, and body force. The body force is the total of external force which is experienced by the body of fluid. It is generally arises from the earth's gravitational field.

When equation 2.6 is applied for the creeping flow ($Re_p < 1$) case, the equation becomes stokes equation which is given by:

$$-\nabla p + \mu\nabla^2\vec{u} = 0 \tag{2.7}$$

The equation neglects the inertia terms which brings non linearity to the equation, thus the solution can be derived analytically. However, many cases in fluid mechanics is involving inertia effect. Oseen suggested an improvement for the solution of Stokes equation to consider the inertia in the far field. Oseen equation is defined as:

$$-\rho\vec{U}\cdot\nabla\vec{u} = -\nabla p + \mu\nabla^2\vec{u} \tag{2.8}$$

in which $\vec{U}$ is the particle's steady velocity. In Oseen equation the frame of reference is moving with the object.

By solving the conservation of mass and conservation of momentum of the fluid, we can estimate the force exerted by the fluid to particles, (F_f). The total fluid forces F_f related to the particle equation of motion through $F_f = m_p d\vec{U}/dt$, where m_p is the mass of the particles and $\vec{U}$ is the velocity of the particle. One of the example of equation to describe the motion of particles is the so called Basset-Boussinesq-Oseen (BBO) equation. BBO equation describes the motion of particles in an unsteady flow. Complete description and derivation of the equation can be seen in the Maxey and Riley paper [23].

2.2. Lateral Migration of Particle

This section presents a brief introduction to the concept of lateral particle migration. It begins from the early observation of the migration to the recent understanding of the physical mechanism behind the migration based on the previous studies.

The phenomenon of particle migration was first observed as the non-uniformity of erythrocytes distribution in blood flow by Fahraeus and Lindqvist [7] as observed in Figure 1.1. They observed that the erythrocytes were concentrated near the axis of the tube. From this observation, it is predicted that in a suspension flow, there is a tendency for the particles to sustain a lateral migration with a further distance from the inlet. This migration of particles is observed due to fluid exerts a force on the particles in the direction of the tube axis.

The exerted force from the fluid to the particle can be estimated by solving conservation mass (2.5) and momentum (2.6). The problem is that the inertia term brings the non-linearity to the equation which makes it difficult to be solved analytically. Inertia term is the critical component which cannot be neglected because, without the inertia effect, there is no particle migration [4, 9]. The common method to solve this problem is using the matched asymptotic expansion method. The method makes separate analysis using Stokes equation for region close to the particle and Oseen equation for the far field. Both solutions are patched together in order to get the full solution of the flow field. The more detailed description about this method can be found in the papers from Kaplun & Lagerstrom [16] and Proudman and Pearson [31].

The early approaches of the analytical studies using the matched asymptotic expansion were focused on estimating the lift forces that act on a spherical particle in a slightly inertial and in an unbounded flow. Rubinow and Keller [34] used this method to study the motion of a rotating sphere in a viscous fluid with uniform shear. It is found that the sphere will experience a lift force which is given by:

$$\vec{F_{RK}} = \pi d^3\ \rho\vec{\Omega}\times\vec{U} \tag{2.9}$$

In which, d is the diameter of the particle, $\vec{\Omega}$ is the angular velocity of the particle, $\vec{U}$ is the velocity of the particle. When the same method is applied to a poiseuille flow with parabolic velocity profile, the lift force on a sphere at given radial position $\vec{r}$ is given in the following equation [34]:

$$\vec{F_L} = -4\pi d^5\rho U_{max}^2\vec{r}/3R^4 \tag{2.10}$$

From this equation it is observed that the resulting lift force is directed to the axis of the tube when it is applied to poiseuille flow. The similar result was also derived by Saffman [35] and Tollert [41].

In 1962, in the effort to study particle migration, Segré and Silberberg [38] conducted an experiment to capture images of neutrally buoyant particles flow inside a circular tube and observe their radial position distribution. This study shows that the particles accumulate and form an annulus at about 0.6 of radii of the tube. The phenonmenon is called as the Tubular Pinch Effect. This result indicates that the particle will migrate to the region between the tube axis and wall not at the axis. It is suggested that the previous theoretical results from Rubinow and Keller is incorrect or incomplete because it is unable to predict the motion of particles away from the tube axis.

In order to investigate Segré and Silberberg result, Oliver [26] reported an experimental result of the movement of a spinning sphere in a vertical tube. It is reported that the particle migrates outward in the direction of the wall to the equilibrium position. The equilibrium position is in the range of non-dimensional radial position (r/R) 0.5-0.65 which agrees with Segré-Silberberg result. This result indicates the existence of a dominant lift force which is directed outward to the tube wall. As particle move to the wall, this force will be balanced by wall repulsion force.

The presence of the wall was reported to resist the movement of particle migration. From the distribution of the lateral force from Ho and Leal in Figure 2.1, it is shown that there is a high lateral force close to the wall which acts in the direction of the tube axis. Saffman [36] explains that the presence of the wall acts on particles in two ways. First, the presence of the walls gives the extra drag to the particles which makes the particle lag behind the flow. Secondly, the region near the wall is dominated by viscous effect; thus the flow field around the particle will differ from the tube axis.

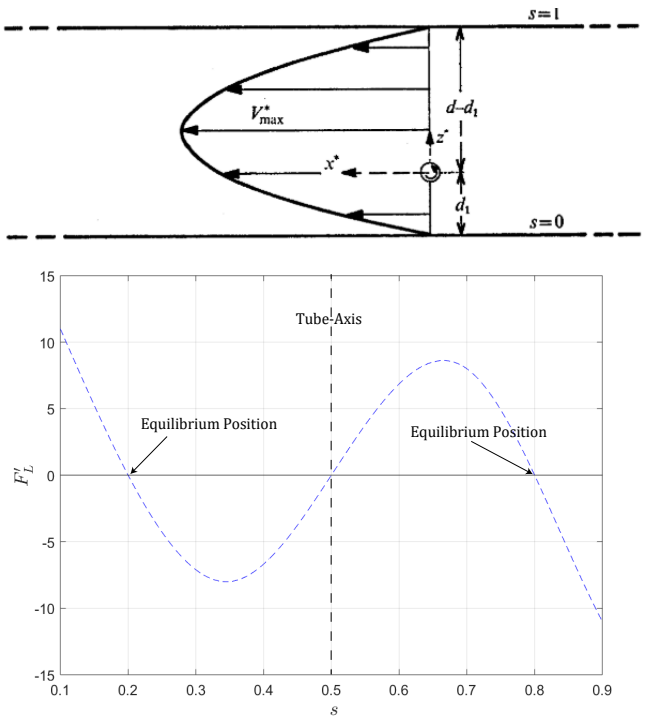

Figure 2.1: The graphic presents the distribution of non-dimensional lateral forces F'_L along the radial position s from Ho and Leal [12]. It is observed that region near the wall will have high lateral force in the direction of the tube axis.

The advancement of computer technology has brought a new approach to study the phenomena in fluid mechanics. It offers methods such as Finite Element Method (FEM), Finite Difference Method (FDM), and Finite Volume Method (FVM) to discretise the governing equation in order to solve it. Still, there is a limitation regarding the computational power to solve complicated cases, especially for the multiphase flow cases. Therefore, the first utilisation of the approach is to solve simple multiphase cases.

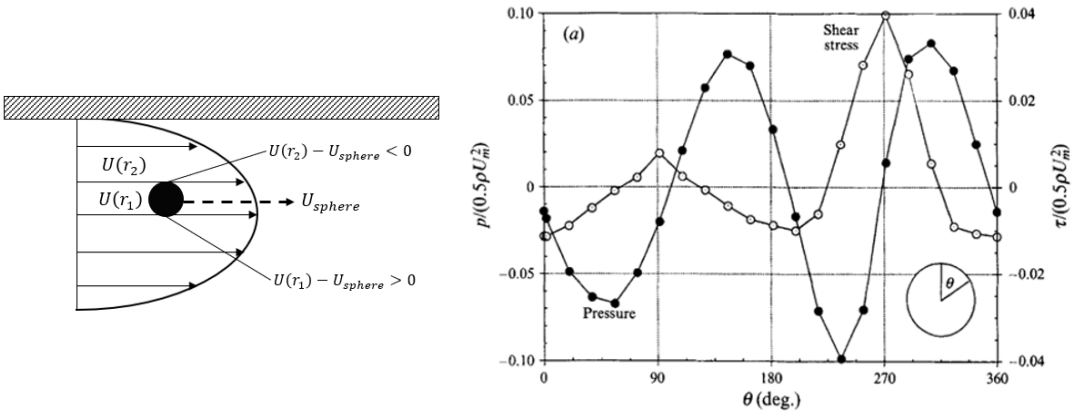

Figure 2.2: (Left-Figure) Concept of lift force due to Poiseuille velocity profile, the surface of the particle at the wall-side (lower bulk flow velocity region) has lower relative velocity compared to the surface of particle at the tube-axis side. This condition will create a lower average pressure on the wall-side compared to tube-axis side which generates a lift force due to the pressure difference between these sides. (Right-Figure) The non-dimensional pressure $P/(0.5\rho U_m^2)$ and shear stress $\tau/(0.5\rho U_m^2)$ distribution around the sphere surface . There is a pressure difference between the third and fourth quadrant of the surface of sphere. Figure is reproduced from Feng et al[8].

.

In the particle migration study, the computational simulation was used by Feng et al.[8] using Direct Numerical Simulation (DNS) to study the movement of spherical particles under Poiseuille flow at Reynolds number high enough to allow the particle migration to occur. It was reported that the particles in Poiseuille flow will experience a lift force generated by the curvature shape of the Poiseuille flow velocity profile. The concept of the lift force can be explained schematically in Figure 2.2. The lift force is generated because lower pressure at the wall-side particle's surface compared to the tube-axis side. Low pressure region is created due to relative velocity between the particle and the flow will be higher at the wall side compare to the axis-side of particle's surface. Therefore, the particle moves toward the wall of the tube due to the pressure difference. The argument is validated from the simulation result of pressure distribution along the spherical particle surface, as shown in Figure 2.2. The significant pressure difference can be observed between the third and fourth quadrant of the surface of the sphere.

To be concluded the physical mechanism of the lateral migration of the neutrally buoyant particle in Poiseuille flow is due to the balance between two forces; Firstly, the lift force in the direction of the wall which is generated because there is pressure difference on the sphere surface due to the curvature of velocity profile. Secondly, the repulsion force from the wall which resist the particles to touch it.

2.3. Research of the Particles Lateral Migration

This section presents the important research on the development of the particle migrations and the effect of particle concentration in the suspension to the migration which are relevant to the study in the thesis project.

2.3.1. The Inertial Effect

One thing that we can learn up to this point is there is no particle migration without the presence of inertial effect [4, 9]. The experiments performed by Segré & Silberberg[38], Oliver[26], Repetti & Leonard[33], and Jeffrey & Pearson[15] confirms that the particle migration occurs at relatively high Reynolds number (below the transitional regime). This importance of the inertia terms makes things complicated for the analytical approach to study the migration because inertia term brings the non-linearity in the equation. Therefore, a simplification with relevant physical reasoning is needed in order to use the analytical approach.

As mentioned before,the early approach to analyze the particle lateral migration was using the matched asymptotic expansion. Cox and Brenner [6] used the method to analyze the lateral migration of a spherical-particle in Poiseuille flow. This report is considered as the first attempt to study analytically the migration in complete three-dimensional Poiseuille flow. A formula were obtained to explain the lateral migration of spherical particles in laminar Poiseuille flow but it is not in an explicit form and cannot solve the direction and magnitude of the lateral force at any given radial position. Even the presence or the absence of the equilibrium position cannot be predicted.

Ho and Leal [12] used a similar approach with Cox and Brenner, They were able to estimate the direction and the magnitude of the lateral force which acts on the neutrally buoyant sphere until it reaches the equilibrium position. In the same report it is stated that the force balance on the spherical particle is not generated instantly at the beginning of the tube. It takes some distance from the inlet for the particle to reach the equilibrium position — the trajectory of the particle migration is presented in Figure 2.3, The trajectory agrees with the experimental results from Tachibana [40].

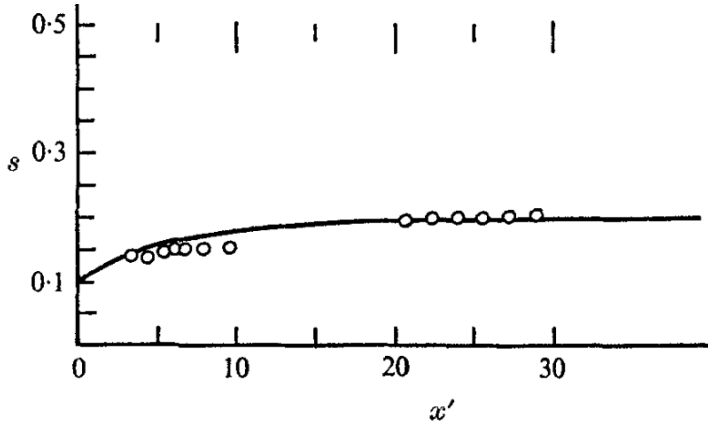

Figure 2.3: The theoretical trajectory of single particle migration under Poiseuille flow from Ho and Leal [12]. The trajectory is compared to the experimental result from Tachibana [40] (marked by circle). The ordinate,s, is the radial position of particle $s = 0$ is the tube wall and $s = 0.5$ is the tube axis. The abscissa is the non-dimensional axial position of the particles $x'[(\rho U_m d/\mu_0)(d/D)^3]$. The Figure is reproduced from Ho and Leal [12]

.

The previous mentioned papers [6, 12] performed the analysis for the case of a spherical particle at relatively low Reynolds number (Re<100). A study in higher Reynolds number is important because the application of the suspension flow is not limited for low Re. Schonberg & Hinch [37] and Asmolov [1] conducted an analysis using the matched asymptotic expansion method to study a motion of neutrally buoyant spherical particle confined by two infinity walls at high Re up to 2000. Both studies were reported that the equilibrium position moves closer to the wall with higher Re. The lift force which brings the particle to the equilibrium position is increasing with Reynolds number. This increase is the reason behind the shifting of equilibrium position closer to the wall compared to the previous result from Segré & Silberberg.

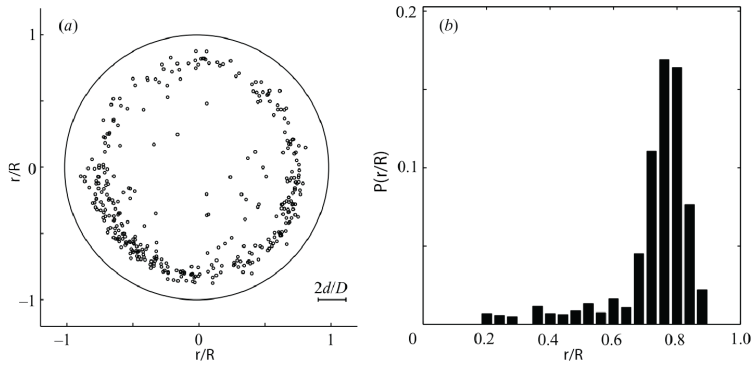

Figure 2.4: Probability Distribution of particle radial position ($P(r/R)$) based on Matas et al. [22]. Figure is reconstruction from Matas et al.[22]

The results from Schonberg & Hinch and Asmolov was confirmed experimentally by Matas et al.[22]. They studied the inertial migration of a dilute suspension under tube flow from the particles radial position distribution. The result is presented in Figure 2.4 in the form of the probability distribution of particles located at a given radial position, $P(r/R)$. From the probability distribution, it is observed that the equilibrium position of particle migration is shifted to the radial position at about $r/R = 0.8$ for $Re > 200$.

Besides the equilibrium position shifting, Matas et al.[22] also reported the relation of the Reynolds number to *migration-distance* which is the distance where all the particles have concentrated at the Segré-Silberberg equilibrium position. They studied this relation by solving theoretical solution from Asmolov [1] using computational simulation. Their result predicts that the migration-distance decreases with an increase in the Reynolds number. It means that the particles will be focused at the equilibrium position in a shorter distance from the inlet at higher Re. This result corresponds to the increase in the lift force which acts on the particles as Reynolds number increases.

In contrast with Matas et al.[22], Morita et al.[25] reported that with an increase in Reynolds number the migration-distance is increasing. They experimented with a dilute suspension in multiple observation distances from the tube inlet to see the evolution of particles radial distribution with the distance from the inlet. It was observed that with higher Reynolds number, at the same distance from the inlet, the probability to find the particles at the equilibrium position is lower. This result indicates that the migration distance increases with Reynolds number. They also proposed an illustration of the migration process as presented in 2.5. All the particles which are initially distributed at random position along the tube cross-section will first migrate inward; then it started to migrate deliberately outward toward the equilibrium position.

Early conclusion of the source of this discrepancy can be directed to the effect of particle concentration on the distribution of particles. Matas et al.[22] studied the relation between the migration length and Reynolds number from the analysis of a single particle, while Morita et al. experimented in a dilute suspension. As will be discussed later, the presence of other particles in the tube disturb the migration of the particle to the equilibrium position. With an increase in concentration, the particles will reach the inter-particle distance which the hydrodynamic interaction between them is significantly affected the dynamics of the particles.

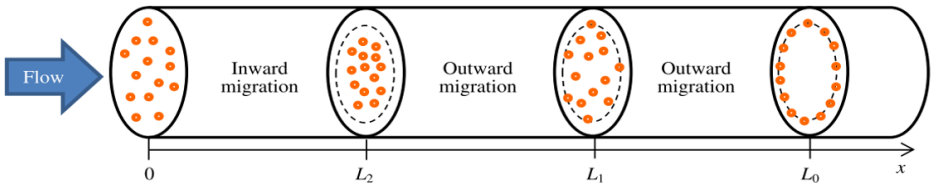

Figure 2.5: Particles distribution development along the tube length . L_2 is the length where most of the particles migrate toward the tube axis, L_1 is the length where the outward migration started to appear, and L_0 is the length where the migration is fully developed, which all the particles have migrated to the equilibrium position. Figure is reproduced from Morita et al.[25]

.

2.3.2. Particle Concentration Effects

Particle concentration is an important parameter to describe the dynamics condition of a suspension flow. The effect of particle concentration on the suspension flow in a circular tube was studied by Karnis et al.[17] using hand-analysed cinematography. From the report, a change in the shape of velocity profile is observed when the particle concentration of the suspension is relatively high. The change is observed from parabolic shape into a blunted parabolic shape. Koh et al.[18] was confirmed the change in velocity profile through laser doppler anemometry (LDA) experiment. It was suggested that the blunting is due to the accumulation of particles at the centre of the tube. The blunted velocity profile is not evident until ϕ>20%. From the same report, it is observed that the accumulation of particles at the tube axis is increasing with particle concentration.

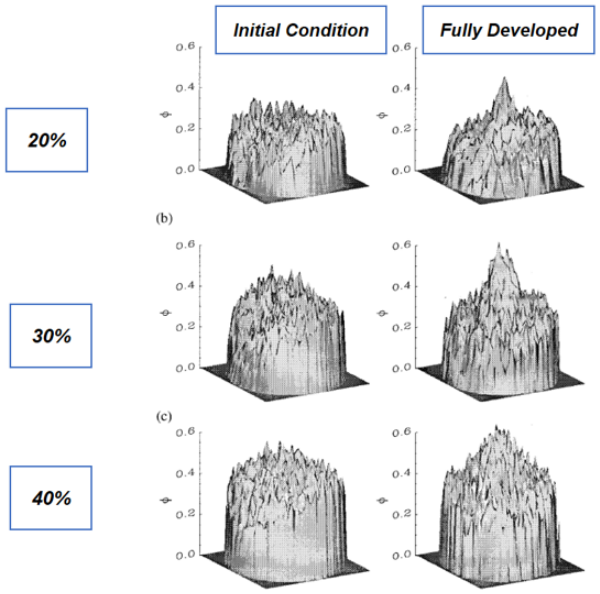

Figure 2.6: Experiment using Nuclear Magnetic Resonance shows that with an increase in particle concentration (20-40%) the fraction of particles at the tube-axis in fully-developed condition is increasing. The Figure is reconstructed from Hampton et al.[10]

.

Leighton and Acrivos [19] reported that the accumulation of the particles in the centre-line is due to the interaction between particles. It was observed that when there is an interaction between two particles, the dynamic of the flow around it will be altered. The presence of the third particle can alter the hydrodynamic interaction into a more chaotic manner for the flow field around them.

The particles radial distribution at the varying level of Reynolds number was studied by Hampton [10] and Han et al. [11] using a nuclear magnetic resonance (NMR) machine. Hampton reported the distribution of particles radial distribution for ϕ = 20-60% as can be seen in Figure 2.6. The particles tend to concentrate in the tube axis with an increase in ϕ. The accumulation of the particles at the tube axis is highly affected by the bulk flow Reynolds number, the higher the Reynolds numbers the particles are more dispersed through the tube cross section. This is an indication that the particle distribution is still affected by the inertia even at high particle concentration. Segré-Silberberg equilibrium position is still evident even at $\phi > 20\%$. Figure 2.7 shows the results from Han et al. The presence of Segré-Silberberg equilibrium position can be seen as a local maxima at particles radial distribution at a radial position about $r/R = 0.5 - 0.6$ which is marked in Figure 2.7. At even higher Re_p, the local concentration of particles around to the Segré-Silberberg equilibrium position is increasing.

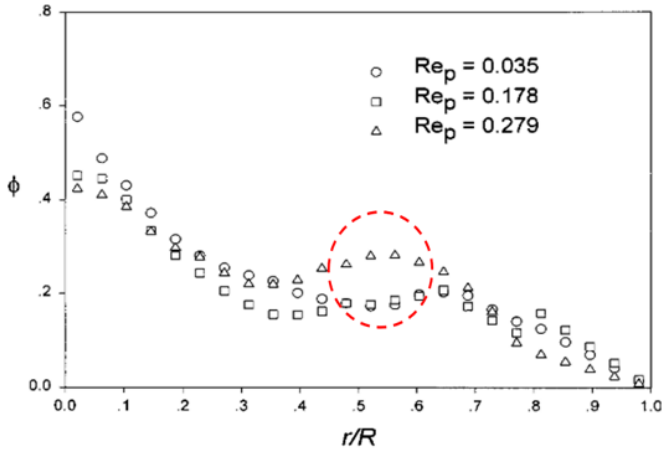

Figure 2.7: Distribution of particles along the radial position at varying Re_p for particle concentration (ϕ) > 20%. This result indicates that even at high ϕ the accumulation of the particles at the Segré-Silberberg equilibrium position is still present as marked by the dashed-circle. The Figure is reconstructed from Han et al. [11]

.

Beside experimentally, the effect of particle concentration to the particle migration is also studied using numerical simulation. Due to the limitation in the computational power, most of the studies are limited at a low particle concentration regime ($\phi < 5\%$). Shao et al. [39] studied the effect of hydrodynamic interaction on the migration by varying the inter-particle distance (δ). It was noticed that the hydrodynamic interaction between particles stabilize the position of the particles at the Segré-Silberberg equilibrium position. A lower δ (higher ϕ) leads to the suppression of the occurrence of the inner annulus. The train like structure was also recognized in the results. It was found that at high ϕ and $Re > 1000$ the train breaks up due to the collision between the particles.

Another study on the effect of particles concentration using computational method was done by Pazouki et al.[28]. The simulation was conducted at $\phi = 0.1 - 3.5\%$. Particles appear to spread along the cross-section of the tube for higher ϕ. The report indicates that the spread of particles at the higher particles concentration because of two reasons; Firstly, the Interaction between particles in the form of drafting, kissing and tumbling, which prevents the particles to coalesce at the narrow annulus. Secondly, a smaller particle distance leads to hydrodynamic interaction between the particles through the wake generation which slows down the migration into the equilibrium position. The slowing down of particle migration can be seen in Figure 2.8 where a comparison of particle trajectories at different distance between particles δ is presented. The number on the curve is the non-dimensional ratio of the distance between particles over the particle diameter δ/d. The simulation was done with the same particle diameter, so a decrease in the number on the curve indicate a decrease in the distance between particles. It is observed that with a decrease in distance between particles, it takes longer for the particle to reach the equilibrium position.

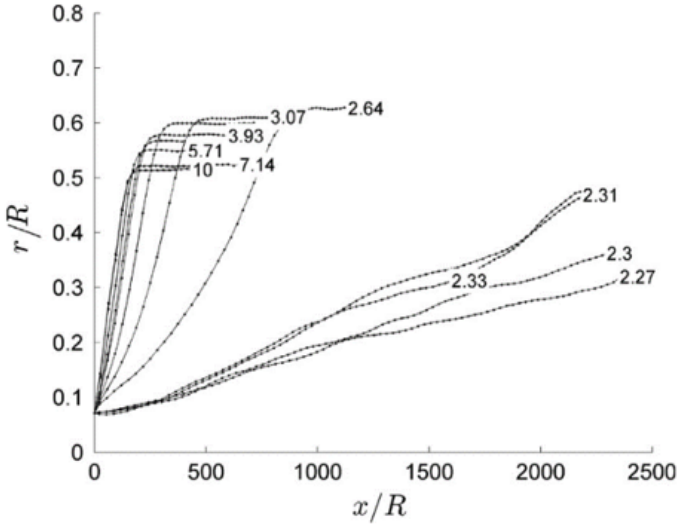

Figure 2.8: The effect of distance between particles to the development length where the particles reach the equilibrium position. The number on the plot is the ratio of the distance between particles and particle diameter. It follows that with smaller particle distance (higher ϕ) the development length become longer. Figure is reproduced from Pazouki et al. [28]

.

Besides affecting the migration, the presence of suspended particles in the flow can also alter the transition of fluid regime from laminar to turbulence. Matas et al.[20] examined the effect of suspended particles on the transition of the flow regime. The presence of the particles in the flow changes the transition Reynolds number, it depends on the ratio of the tube diameter (D) to the particle diameter (d). For $D/d > 65$ the transition is shifted to $Re > 2100$ while for $D/d < 65$ the transition behaviour depends on particle concentration. For ϕ<10% the transition is shifted into lower Reynolds number, while for higher particle concentration, the transition Reynolds number increases with ϕ.

2.3.3. Secondary Phenomena of the Particle Migration

Inner Annulus

From Matas et al.[22], an interesting phenomena was reported, which at $Re > 600$ second equilibrium position is present, as shown in Figure 2.9. The location of this second equilibrium position is at a radial position between the centre-line of the tube and the Segre-Silberberg equilibrium position. Due to its location, the annulus is named as *the inner annulus*. The presence of the inner annulus is a new discovery in the particle lateral migration study because it was not predicted from the previous theoretical analysis by Asmolov [1] and Schonberg & Hinch[37].

Matas et al. analyzed the occurrence of the inner annulus from the distribution of lift forces that acts on a sphere along the radial position as shown in Figure 2.10. The distribution of the lift forces was calculated numerically by solving the solution from Asmolov [1]. The distribution shows that with an increase in Reynolds number the lift force distribution of the lift forces is flatten. Even though the lift force distribution seems flat, if it is looked carefully for $Re = 1000$, there exists a local minima of lift force at a radial position about $r/R = 0.4$ and local maxima at at a radial position about $r/R = 0.85$. If the lift force distribution results are matched to the probability distribution of particle radial distribution results, it is shown in Figure 2.10 that the inner annulus is located around the local minima position. They concluded that the appearance of the inner annulus is due to the particles have insufficient lift force to surpass the local maxima which are located at the Segré-Silberberg equilibrium

position. The inner annulus is also reported to have stability at transition flow regime. It is observed that at $Re = 1600$ only the inner annulus retained as the equilibrium position. Thus, they concluded that the inner annulus is a real equilibrium position rather than a transient phenomenon.

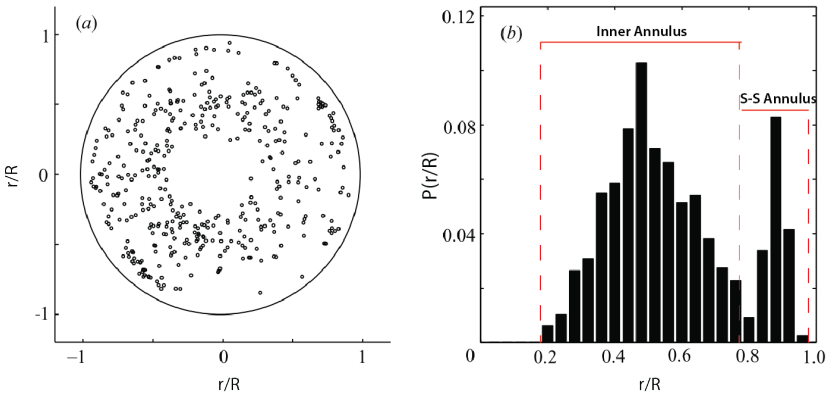

Figure 2.9: The appearance of the Inner Annulus in Matas et al. [22] results. The presence of the inner annulus is manifested by the appearance of two peaks as shown in the right-hand side figure. Figure is reconstruction from Matas et al. [22]

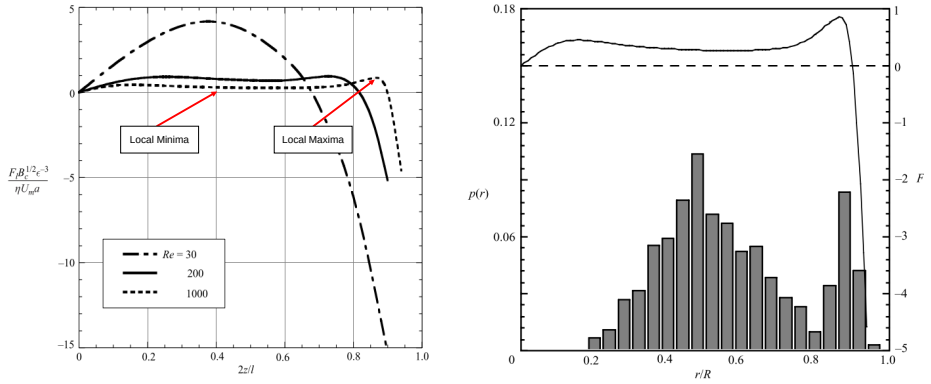

Figure 2.10: Radial forces distribution along the tube radius. (Left-Figure) The distribution of the lift force acted on a sphere. The oordinate is the non-dimensional lift-forces acted on a sphere ($F = F_l R_c^{1/2} \epsilon^{-3}/(\mu U_m a)$), where R_c, is the tube reynolds number, and $\epsilon = (0.5 Re_p)^{1/2}$ and the abscissa is the non-dimensional radial position where z is the distance from the tube-axis and l is the diameter of the tube. Figure is reproduced from Matas et al. [22]

.

The discovery of the inner annulus is followed by the reluctance that it is only a transient phenomenon. Morita et al.[25] experimental result in Figure 2.11 indicates that an increase in the non dimensional distance from the inlet (L/D) the probability to find the particle in the inner annulus (P_i) is decreasing. On the contrary, the probability to find particles in the Segrè Silberberg annulus (P_{Outer}) is increasing. Morita et al. argued that the inner annulus could be considered as the second equilibrium position. They concluded that the inner annulus is just a transient phenomenon before particles reach Segré-Silberberg equilibrium position.

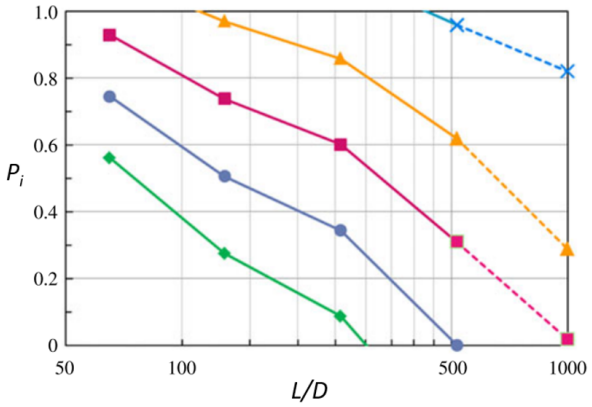

Figure 2.11: Probability to find particles in inner annulus (P_i) will decrease with a further distance from the tube inlet at D/d=12, for Re = 200 (diamonds), 400 (circles), 600 (squares), 800 (triangles), and 1000 (cross). Figure is reproduced from Morita et al. [25]

.

Trains of Particles

Trains of particles, as can be seen in Figure 2.12, is the phenomena where several particles are aligned in the direction of the flow and form a line which looks like a train structure. The alignment itself is a result of the hydrodynamic interaction between the particles due to the flow field condition around them.

The formation of trains of particles is briefly mentioned in Segré-Silberberg report [38] as ”chains” of particles when the concentration of particles increased. Matas et al.[21] systematically studied the formation of trains of particles through the experiment at varying Re and particle sizes. It was found that with higher Re, the number of particles in the trains increases until it reaches a peak point then the number of particles on the trains is decreasing afterwards. The decrease in the number of particles in the trains after passing a particular value of Reynolds number is highly related to the formation of the inner annulus. From the previous section, it is reported that the inner annulus starts to appear at Re around 600, which from Figure 2.13 is the point where the number of particles in trains starts to decrease. From the experiment observation, the trains will not be formed at the location of the inner annulus.

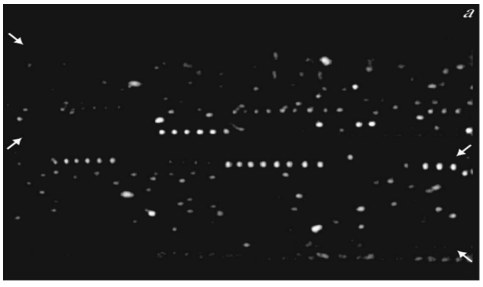

Figure 2.12: Image of Trains of Particles. Figure is reproduced from Matas et al. [21]

.

From the same report, the mechanism of the trains formation was studied through numerically determined flow field around a particle in the trains for Re_p=0 and Re_p=10. An important observation from the flow field analysis is the appearance of a closed streamline region around the particles as can be seen in Figure 2.14(a.). For an increase in Re_p, the closed streamline collapses which result in an open and reversing streamline region as shown in Figure 2.14(b.) pointed by the arrow. The neighbouring particles will be trapped in this reverse streamline region to form a train like structure. The size of the reversing streamline

region decreases with an increase in Re_p. This relation is implied that the distance between the particles in the train is decreasing with an increase in Re_p.

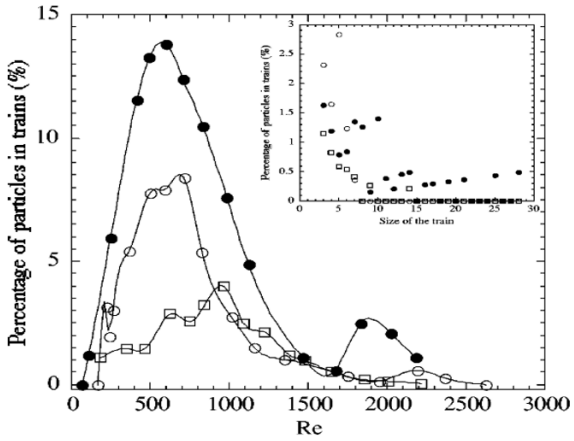

Figure 2.13: Percentage of particles in trains vs Reynolds number at different particle sizes, D/d= 17(open-circle), 19(filled-circle), 33(open-square). Figure is reproduced from Matas et al[21]

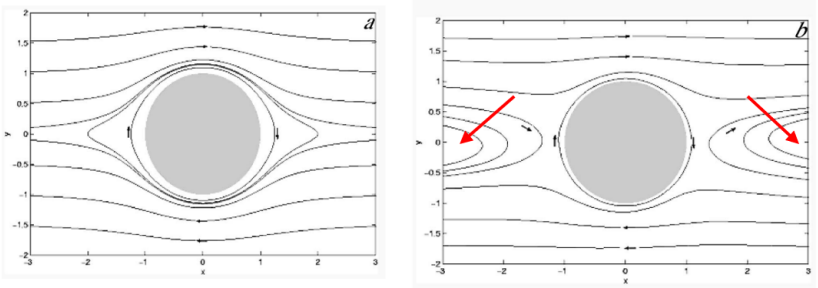

Figure 2.14: Streamline around single particles (a.) Re_p=0 the closed streamline is observed in the flow field. An increase in Re_p can cause the closure breaks up as shown in figure (b.) for Re_p=10 and reverse flow region is created (pointed by arrow). Figure is reproduced from Matas et al.[21]

Matas et al. [21] stated that the trains are mostly located in the Segré-Silberberg equilibrium position, therefore there is an indication of a direct relationship between the particle migration to the formation of particle trains. Thus far, the study of the particle trains was only conducted in one observation distance from the tube Inlet. Morita et al. [25] result indicates the importance to make an observation of particle migration phenomenon in multiple observation distances to see its development. There is a possibility that when an observation is conducted at one distance only, the particle migration is not in a fully developed condition yet and so does the trains formation.

Moreover, there is also a gap in understanding the effect of particle concentration on the formation of trains. The formation of trains is closely related to the hydrodynamic interaction between the particles. However, there has not been any study reported the effect of particle concentration to the formation of particle trains in a circular tube. As already mentioned, particle concentration is crucial for the dynamic condition between particles. This is an indication that it will affect the formation of particle trains.

2.4. Concluding Remarks of The Literature Study

A particle which flows in a shear flow will sustain a lateral migration to the equilibrium position. The migration is due to exerted force from the fluid to the particle. In a Poiseuille flow, the lift force is generated due to the curvature shape of the velocity profile. The pressure difference on the particles surface creates a lift force in the direction of the tube wall. As the particle moves to the wall, the lift force is balanced by the wall repulsion force. This wall repulsion force is a present as a result of different flow regime around the particle near the wall. The balance between these forces results in particle stays in an equilibrium position.

Based on the studies on the effect of Reynolds number to the particle migration, different researchers agree that the migration is highly related to the inertia effect from the flow to the particles. Experimental and Theoretical results have agreed that particle migration is not present in the absence of the inertial effect, as in the case of creeping flow. The lift force that acts on the particles is increasing concerning an increase in Reynolds number; this is evident from the shifting of equilibrium position closer to the wall at a higher Reynolds number. However, there is a dispute about the influence of Reynolds number to the migration-distance. The analytical result shows that the increase in Reynolds number causes shorter migration-distance, while experimental work shows an opposite relation.

Particle concentration in a suspension has been reported to have the opposite effect with the inertial effect. In contrast to the inertial effect, an increase in particle concentration has been reported to suppress the particle migration to the equilibrium position. Instead of migrating to the equilibrium position, particles are concentrated at the tube axis at considerably high particle concentration. The resistance to particle migration at high particle concentration can be either from particle-particle collision or hydrodynamic interaction between particles, depending on the level of particle concentration. This resistance is also affecting the migration-distance, it has been reported from numerical analysis that particle migrates at a longer distance with higher particle concentration. However, the available experimental data is still scarce to confirm this result and derive a general conclusion about the effect of particle concentration to the development of particle migration.

There are two new observed phenomena following the development of particle migration, the occurrence of the inner annulus and the formation of particle trains. Both phenomena are profoundly affected by the variation in the Reynolds number. The inner annulus is reported to start appearing at Reynolds number around 600, while the number of particle trains is gradually increasing with Reynolds number until at some level it is started to decrease. Even though there is a number of evidence on the effect of Reynolds number to these secondary phenomena, there is still a lack of evidence for the effect of particle concentration.

Previous research has indicated potential associations between the axial distance to the development of particle migration. Most experimental studies in the field of particle migration have only conducted an experiment at one observation distance. The advantage of observation at multiple distances from the inlet is the availability to see the development process of the particle migration and study the effect of variation in the experimental parameter to this process.

3

Experimental Technique

This chapter presents the experimental technique which is conducted during the thesis project. Section 3.1 explains the experimental setup which was used in the thesis study. The explanation is divided into two parts, the flow system setup and the optical system setup. Section 3.2 presents the result from the measurement of particles size which was used in the experiment. In Section 3.3 the selection of the experimental parameters such as particle concentration and Reynolds number were defined. Finally, the chapter is ended with the description of the experimental procedure of this thesis study in section 3.4.

3.1. Experimental Setup

3.1.1. Flow System

The flow system of the experimental setup is schematically shown in Figure 3.1. The main part of the flow system is a glass tube which has inside diameters D= 10 mm. There is four glass tube inter-connected with plastic flanges which made 4.8 m length distance from the inlet. In this thesis project, the observation distance was divided into four sections, which were positioned at L/D =150,250,350,450, respectively.

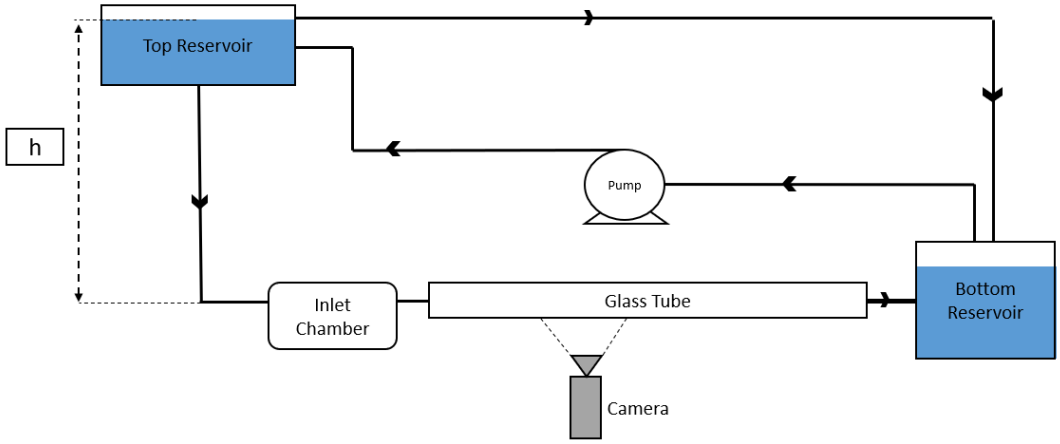

Figure 3.1: Schematic overview of the flow system of the experimental Setup

.

The flow is driven using the hydrostatic pressure, which is controlled by varying the height measured from the water surface in the top reservoir to the height of the tube (h). At the

highest elevation, the maximum Reynolds number can reach $Re = 1500$. The fluid was flowing into the inlet chamber to be conditioned before reaching the glass tube. From the tube, the fluid went into the bottom reservoir to be recirculated by the pump. An overflow system is used to avoid over-filling at the top reservoir by bringing the excess fluid to the bottom reservoir. Figure 3.2 shows pictures of the constructed system.

In an inner flow such as Poiseuille flow, there is a region near the entrance where the flow profile is still disturbed by the growth of the boundary layer. The experiment is conditioned to avoid this flow development effect in the experimental result. Thus, the observation distance has to be longer than the entrance length, L_D, and it is calculated using equation 3.1 for laminar flow [44]:

$$\frac{L_D}{D} = 0.06\ Re \tag{3.1}$$

For the maximum Reynolds number of the setup ($Re = 1500$), the entrance length is calculated at L_D=84 cm.The first observation distance in the experiment is at L=150 cm. Thus, it is free of the flow development effect.

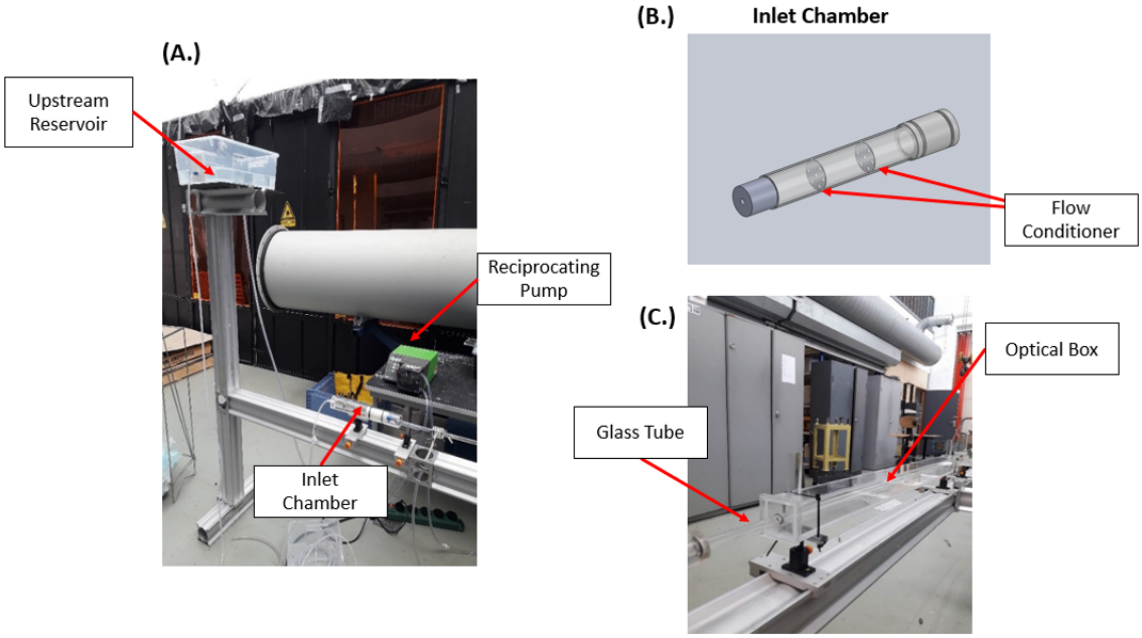

Figure 3.2: Flow system setup for the experimental study, (a.) Upstream reservoir and Inlet chamber, (b.) schematic of the inlet chamber, (c.) Glass-tube covered by optical box.

.

The inlet chamber in the flow setup has a purpose of decreasing the entrance length L_D of the flow. Generally, the mechanism of the inlet chamber to diminish the eddies can be divided into two processes. Firstly, the diameter of the inlet chamber greater than the diameter of the tube from the top reservoir. As a result, there is a decrease in the Reynolds number of the flow. A decrease in Reynolds number means that in the flow the viscous forces becomes more dominant compared to the Inertia forces . As a result, there is an increase in the dissipation of flow eddies. In addition to the eddies dissipation, the inlet chamber also has two flow conditioners to break up larger eddies structure into smaller eddies, which is easier to dissipate. Even though in the thesis experiment at the selected observation distance the flow is already fully developed without the use of the inlet chamber, the experimental setup was designed to have the capability for further study at the higher Reynolds number.

The working fluid is a mixture of salt and water to match the density of the fluid with the density of the particles to create a neutrally buoyant environment as illustrated in Figure 3.3 (a.). Salt was added into the water until the particles were uniformly distributed along the depth of the glass container as shown in Figure 3.3 (d.). This condition is reached when a mixture of salt and water density, ρ=1035 kg/m^3. This density value agrees with the particles density value which is listed in the product specification from the factory.

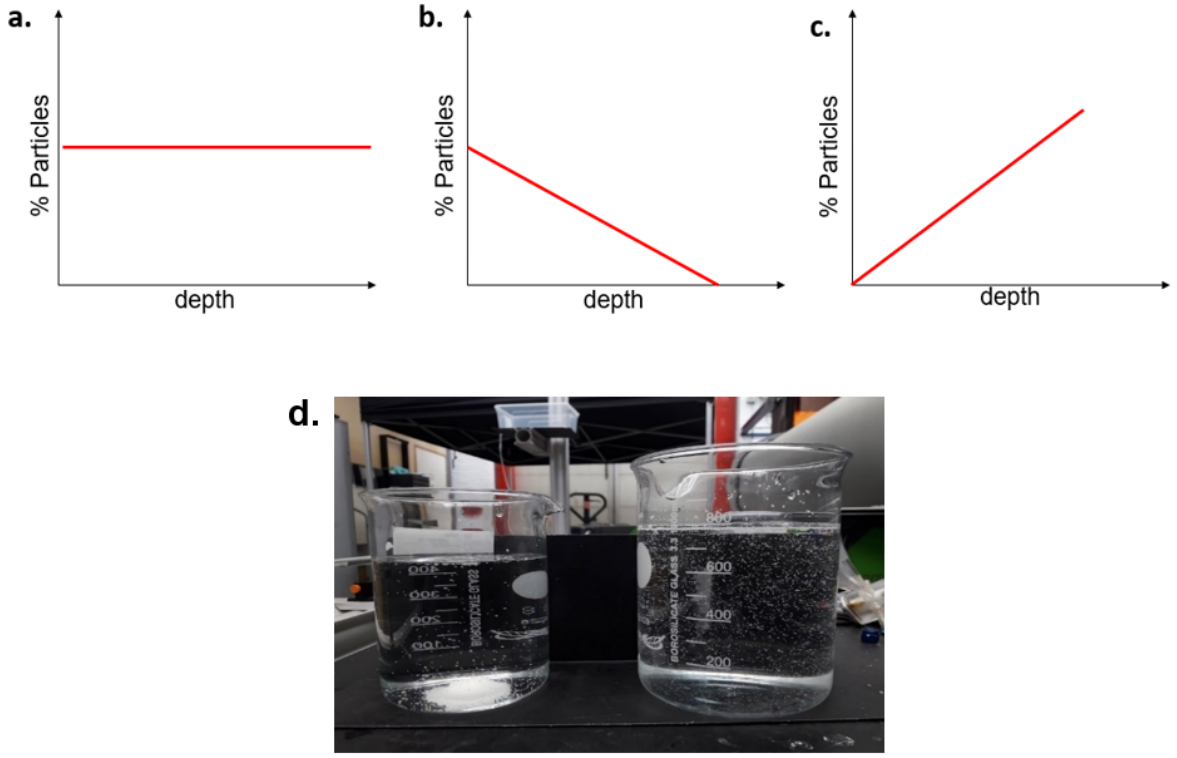

Figure 3.3: Distribution of particles vs the depth of the fluid (a.) neutral buoyancy ($\rho_{fluid} = \rho_{particle}$) , (b.) positive buoyancy ($\rho_{fluid} > \rho_{particle}$) , and (c.) negative buoyancy ($\rho_{fluid} < \rho_{particle}$), (d.) example of neutral buoyancy (right) and negative buoyancy (left).

Table 3.1 summarizes the key parameters of the flow system of the experimental facility in this thesis study. The working temperature value is based on the measurement at the time of the experiment was conducted.

Table 3.1: Summary of the key parameters of the experimental facility

tube inside diameter D	10 mm
total length	4.8 m
total height	2.5 m
Re	0-1500
fluid density ρ	1035 kg/m^3
working temperature	20-24 ^{0}C
fluid viscosity at 24 ^{o}C	$1 \times 10^{-3} Pa.s$

3.1.2. Optical System

The schematic of the optical setup can be seen in Figure 3.4. The optical box is illuminated by two LED panels. The images are taken with a scientific camera (Imager sCMOS) with specifications listed in Table 3.2. The maximum frame per second in the experiment was set

at 25 frames per second to avoid excessive data. The lense that was used in the experiment is a NIKON 35 mm lense with a maximum aperture number (F#) is F#=2. The lense was set at a distance from the object, Z_0=300 mm. This means that the image has a magnification factor, $M = 8.6$, which is obtained from the ratio of the distance from the camera to the object and distance from the lense to the camera sensor. With a camera sensor size at $16.6 \times 14mm^2$, the field-of-view is determined to be $142 \times 120mm^2$. For the optical system configuration, the aperture of the camera mostly set at F# = 4.0 and F# = 5.6. From particle size measurement which will be presented in the next section, the particles have size d = 520 µm and the pixel size of the image of the particles (d_t) is observed to be 9-10 pixels.

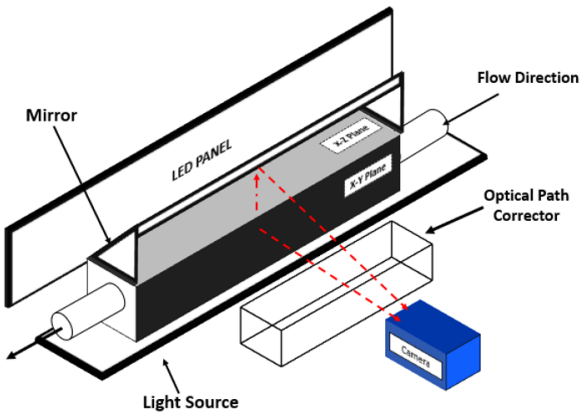

Figure 3.4: Arrangement of the optical system in the experiment setup.

.

Table 3.2: Specification of the Imager sCMOS camera (https://www.thorlabs.com)

Exposure Time	15 μs-100 ms
Digital Output	16 bit
Number of Pixels	2560 × 2163 pixels
Pixel Size	$6.5\mu m \times 6.5\mu m$
Sensor Size	$16.6mm \times 14.0mm$
Frame Rate (max)	50 fps

The optical box is constructed from PMMA with a thickness of 4 mm. It is filled with the same fluid as the fluid inside the tube. The purpose of this optical box is to decrease the effects of optical aberrations, as a consequence of tube curvature. Optical aberration is the condition where the light is not concentrated on one focal point; the light is spread out, which makes the picture blurred. By introducing an optical box, the effect of optical aberration is minimised.

In order to get the information about the position of particles in three different axis, a mirror is placed above the optical box. With this step, two planes of images can be captured, the first plane with the x-y position of the particles, and the second plane with the x-z position of the particles. From both acquired images, the three-dimensional position of each particle can be constructed. Sufficient light sources are needed to produce a sharp image of the particles. Two LED panels are used to illuminate the particles with the arrangement as shown in Figure 3.5.

The application of the mirror will introduce a sharpness problem because the two optical paths are not equal. This application causes one image appears sharp while the other is blurry. An easier solution to this problem is to decrease the camera aperture to create a wider depth of field. However, this solution causes a decrease in the amount of light captured

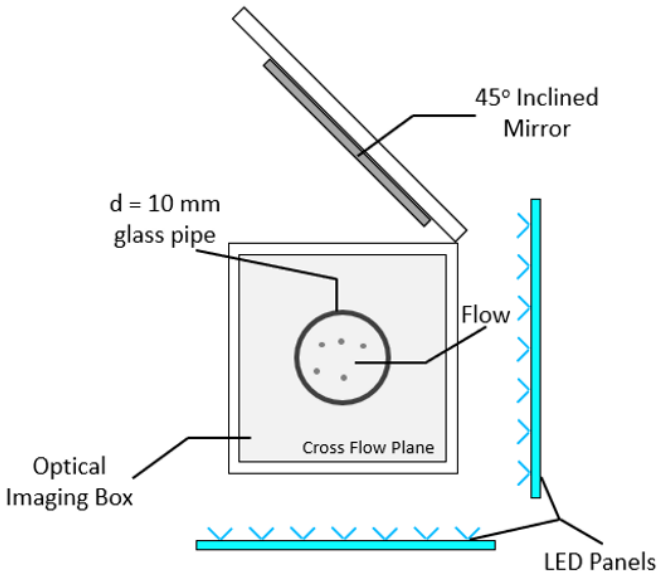

Figure 3.5: Schematic of cross-section of the optical box of the experimental setup. Two LED panels were used to illuminate the particles. Figure is reproduced from Cenk Cetin

.

by the sensors due to the smaller diaphragm opening to the lenses. An alternative is to put a box which is filled with a medium in front of the camera to correct the path of the light. Refraction will bend the light path to lie in the depth of field of the camera. The requirement of the medium thickness (x) can be calculated with equation 3.2 from VanDuin [42]:

$$x = \frac{\Delta L - (n_{pmma} - n_{air})2d_{pmma}}{n_{water} - n_{air}} \tag{3.2}$$

The thickness of PMMA (d_{pmma}) is 5 mm with refractive index $n_{pmma} = 1.49, n_{water} = 1.33$, and $n_{air} = 1$. ΔL is the distance between the top of the optical box to the mirror. The distance was measured to be at about $\Delta L = 40mm$. Water is used as the medium in front of the camera in this thesis project. The required water thickness (x) is calculated to be $x = 107.5mm$. Water was stored in a pool constructed from PMMA with 5 mm thickness and it is placed in front of the mirror plane.

3.2. Particle Size Measurement

Spherical polystyrene beads are used as dispersed particles. A Particle size measurement was conducted to validate the size distribution of the particles. In order to measure the particles size, a microscope integrated with the personal computer was used to capture the images of different specimens. The specimens were a glass plate with several particles placed on the plate.

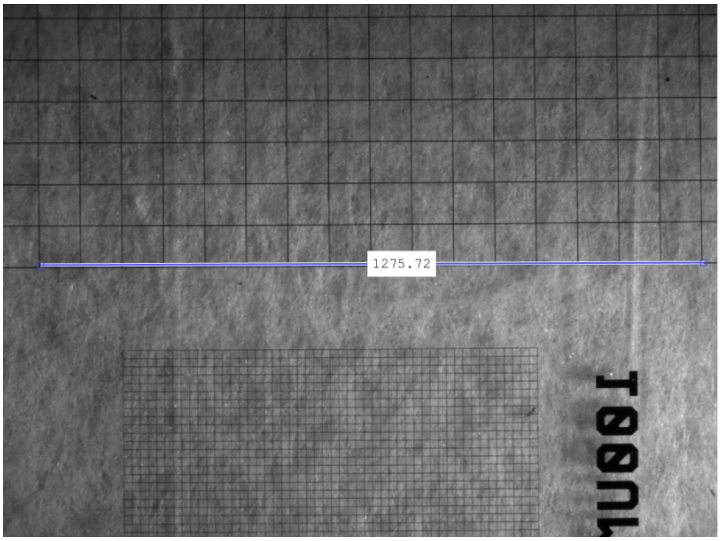

Figure 3.6: Example of the captured image of the calibration plate

Before capturing the images of the specimens, the image of the calibration plate was taken as shown in Figure 3.6. From this image, the size of the pixels can be determined. It followed that for the settings used, a pixel was found to correspond to 6 µm.

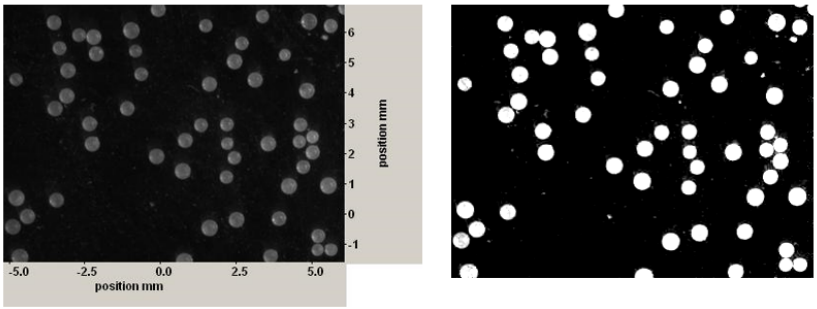

Figure 3.7: The captured picture of a specimen (left) which binarised in Matlab (right) to calculate the diameter of each object.

The next step is capturing the images of the specimens. An example of a specimen image is shown in Figure 3.7. Multiple images of different specimens are captured to ensure the convergence of the measurement results.

Each image is binarised to isolate the image of the particles from the background of the images, as shown in Figure 3.7. The threshold number for binarisation is determined using Otsu's method [27]. The method relies on the histogram distribution of pixel intensity information of the image. Two classes are selected from the histogram, foreground (particles) and background pixels. Then the variance of each classes, foreground class variance (σ_1^2)and background class variance (σ_0^2) is calculated. A threshold is selected by finding the value that minimises the results of equation 3.3[27]. The equation calculates the intra-class variance ω_0 and ω_1, which are the sum of the probability of each class which act as the weighting function.

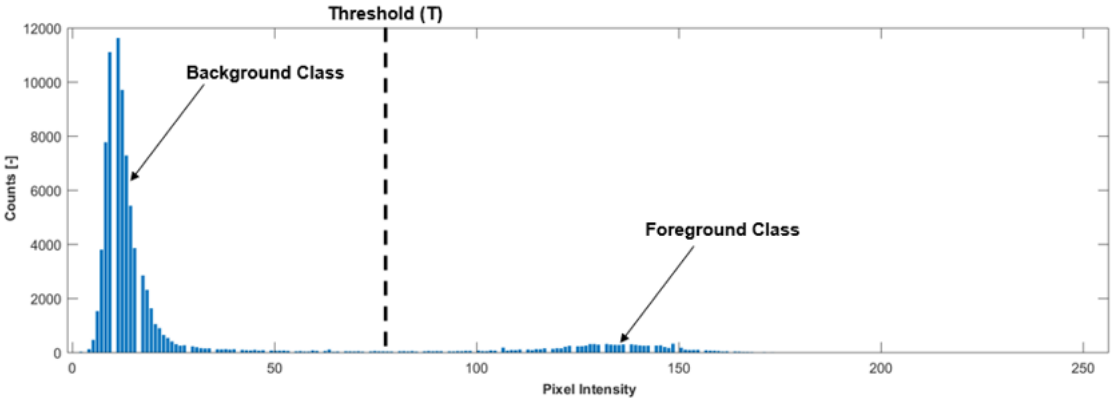

$$\sigma_{\omega}^2(T) = \omega_0(T)\sigma_0^2(T) + \omega_1(T)\sigma_1^2(T)$$
$$\omega_0(T) = \sum_{i=0}^{t-1} pi \tag{3.3}$$
$$\omega_1(T) = \sum_{i=t}^{t-1} pi$$

From the binarised image, the diameter of each particle is determined using the Circular Hough Transform method [45]. The circular Hough Transform method is a technique which detects circular shapes in an image through a voting procedure. The concept of the Hough transform is illustrated in Figure 3.8. The candidate pixels for the voting procedure are the pixels which are located at the boundary of the circle. The high gradient in the intensity value of the pixels is an indicator that the pixel is located at the boundary of a circle. Every candidate pixels will form a circle with a previously estimated fixed radius. From the formed circles, the pixels located at the edge of the circles are accumulated in the array of votes. The location of the most voted pixel is determined as the centroid of the circle.

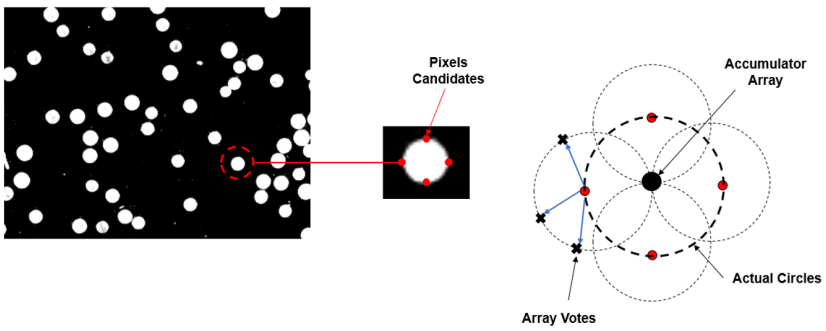

Figure 3.8: Hough Transform Method to detect the circular shape in the image. The pixels which is located at the boundary of the circle act as the voting agent to determine the centroid of the actual circle.

From every image of the specimens, the mean value of the particle image diameter (d_t) is approximately 88 pixels. The particle image diameter value is determined after the calculated mean value converged at one particular diameter value. The particle image size can be converted from pixel to micrometer using the calibration constant from the calibration process. Figure 3.9 shows the results of the measurement in the form of size distribution and convergence graph. The particles image diameter is converged at $d_t = 528\mu m$.

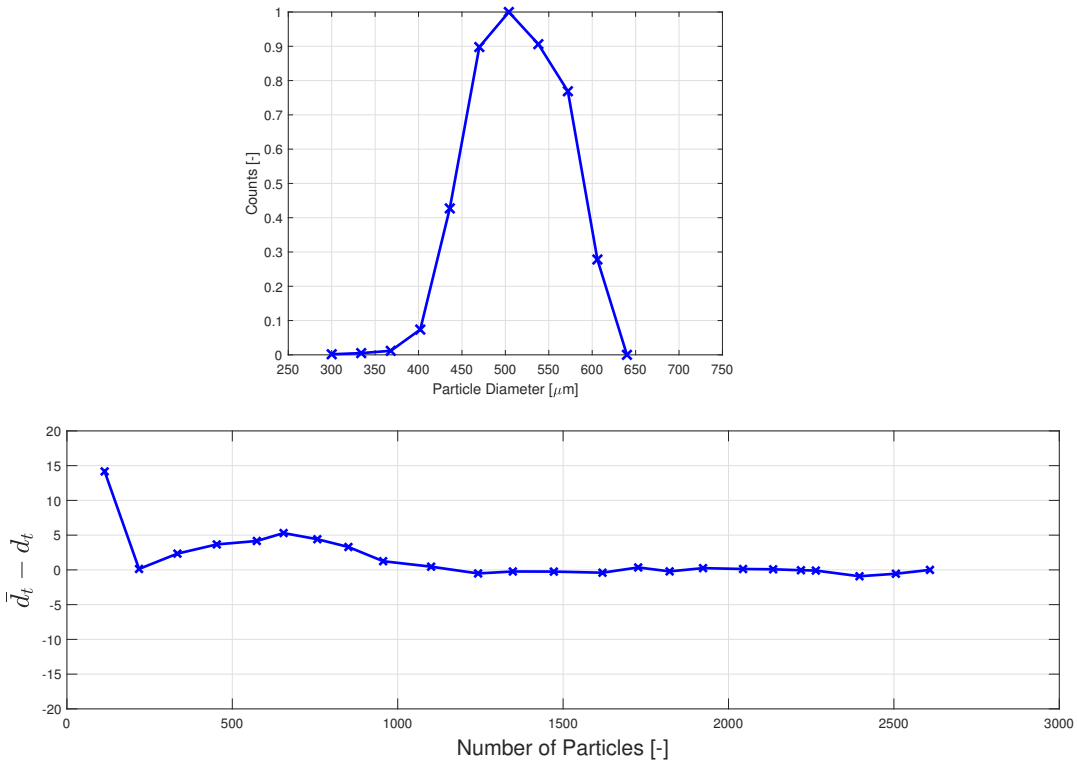

Figure 3.9: The particles size distribution from the measurement results. Particles image diameter (d_t) is converged at $d_t = 528\mu m$

When using an optical measurement system attention should be given to the effect of light diffraction. This effect, as illustrated in Figure 3.10, occurs because the ray of light which initially occupied a wide space goes through the lense opening. As a consequence, it will make the light slightly bent. Initially, each ray travels at the parallel distances, due to the bending, the distance will be different. As a result, the so-called airy disk formation is formed. The width of the airy disk is the maximum theoretical resolution of the optical system, also called the diffraction limited image diameter (d_s). This Diffraction effect can overestimate the measurement results due to the formation of the airy disk.

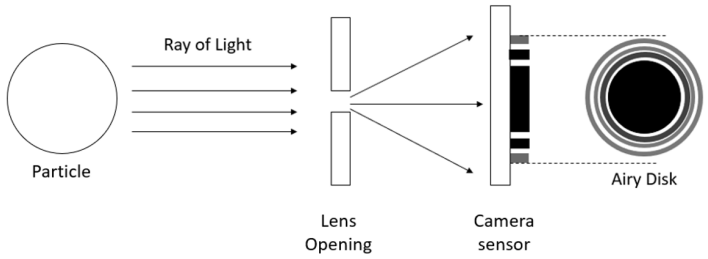

Figure 3.10: The illustration of the diffraction effect which creates the Airy Disk structure at the particle images which causes overestimation in the size measurement result.

The diffraction limited image diameter can be calculated using equation 3.4 from Raffel et al.[32] where F# is the aperture number, M is the magnification factor, and λ is the wavelength

of the light source.

$$d_s \approx 2.44F\#(M+1)\lambda \tag{3.4}$$

The measurement was conducted with F# =0.28, M = 11.4 and a light source with a wavelength of approximately 520 nm. This condition yields (d_s) equal to 4.4 µm. It means that the measurement results are overestimated with approximately one pixel due to diffraction. The optical system has a pixel size approximately 6 µm, using equation 3.5 from Raffel et al. [32] the particles have diameters, d = 520 µm.

$$d_t = \sqrt{(Md)^2 + d_s^2} \tag{3.5}$$

The effect of the pump in changing the shape and the size of the particles was investigated. The investigation is done by measuring the size of the original and used particles. The result is shown in Figure 3.11 for both batches. The distribution shows that there is no significant difference in size between the original and used particles. For the shape of the particles, the investigation was done by observing the roundness of the used particles from the captured images. It can be concluded that the pump does not affect the particles shape and size.

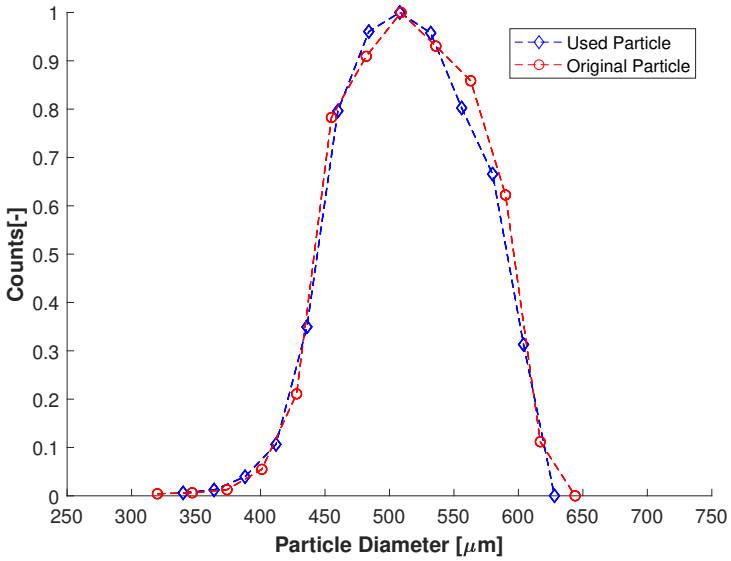

Figure 3.11: The particle distribution size of the original particles (circle) and the used particles (diamond). The distribution shows that the pump has only small effect to the particle size.

3.3. Experimental Parameter

This thesis project, focuses on the effect of the concentration and Reynolds number on the lateral particle migration. The range of these experiment parameter can be seen in Table 3.3.

Table 3.3: The Experimental Parameter Variation

Re	200
	500
	1200
Particle Concentration $\phi(\%)$	0.01
	0.05
	0.1
	0.5
	0.8
	1.6
Observation Distance (L/D)	150
	250
	350
	450
Frame per second (FPS)	10 for $Re \approx 200$
	15 for $Re \approx 500$
	25 for $Re \approx 1000$

Three different Reynolds number is chosen, Re=250, 500, and 1000. These numbers are chosen because at these numbers the phenomena such as inner annulus and trains of particles were started to occur. This thesis does not aim to study the particle distribution at the turbulence regime, maximum Re is chosen at 1200. From Matas et al. [21], the presence of the particles in the fluid can bring the transition Reynolds number into a lower value of Re. Therefore, the experiment was not conducted at Re > 1200 to prevent the change in the flow regime affect the analysis of the results.

The particle concentration is chosen to be varied at a relatively low concentration. It is because of the limitation in the experimental method to study at a high particle concentration. Particle concentration was selected to start from $\phi = 0.01\%$ because when the experiment was conducted at $\phi < 0.01\%$ the number of the particles in each frame will be very low. As a consequence, a large number of frames needed to prevent high uncertainty in the experiment result. However, only at $\phi = 0.05\%, 0.1\%$, and 0.5% which the experiment was conducted at all observation distance (L/D).

The frame rate of the camera (FPS) is adjusted concerning the flow rate. In this case, it is fixed based on the bulk flow Reynolds number Re. The higher the Reynolds number the frame rate has to be higher to accommodate the higher speed of the particles. When the Reynolds number is lower, the frame rate is adjusted into a lower rate to avoid excessive data is stored.

3.4. Experimental Procedure

For every single measurement at different L/D, the experimental procedure is repeated. The particle concentration is held constant until the measurement at all L/D is conducted for each Re. The procedure is divided into three steps, pre-recording, recording, and post-recording. The recording process is done with image processing software from LaVision (Davis 8.1) which is directly connected to the camera during the recording process.

For every experiment, 2000 frames were recorded corresponding to 40 Gigabytes size of data. As will be presented in the next chapter, the number of particles captured varied with a variation in particles concentration.

The frame rate of the camera has to be able to capture the position of the particles in motion. Therefore the rate has to be higher than the maximum velocity of the particles at any given Reynolds number. The frame rate is adjusted to the Reynolds number of the observation, as listed in table 3.3.

Pre-Recording :

- Before performing measurement, the temperature and the density of the working fluid are measured using thermometer and hydrometer respectively.
- The fluid density is held constant through the experiment, if there is a change in the density of the fluid the working fluid must be altered by adding the salt or water depending on the change in the density.
- The top reservoir is positioned at a particular height with respect to the tube inlet position, depends on the Reynolds number of the experiment.
- The mass flow rate is measured at the end of tube, then the mean velocity (U_m) is calculated using equation 3.6. $\dot{m}$ is the mass flow rate which is measured at the outlet of the tube. From the calculated U_m, the Reynolds number of the experiment can be calculated using equation 2.1.

$$U_m = \frac{\dot{m}}{\rho \pi R^2} \tag{3.6}$$

Recording:

- The image quality of the image is checked, especially the focus quality and the exposure of the images from the live preview on the monitor. If the images appear with low focus quality, the lens aperture is adjusted until the image sharpen. In this experiment the lens aperture was only varied between F#= 4.0 and F#=5.6.
- The brightness of the image is adjusted by setting the shutter speed of the camera in the Davis 8.1 software to give a suitable exposure level. In this experiment, the shutter speed was set at 1/1500-1/2000. Beside an effect on the intensity of light on the image, the shutter speed also affects the ability of the camera to capture the image. When the shutter speed is too slow, motion blur might appear to the image of particles.
- The Frame rate is adjusted to match with measurement Reynolds number as shown in table 3.3.
- The frame without the particles in the pipe is recorded as the reference frame for background subtraction.
- The images is recorded (2000 frames) for every change in parameter.

Post recording:

- The images quality is checked again to ensure that the quality is sufficient for image processing.
- The images is exported to TIFF format.

4

Experimental Data Processing

This chapter presents the processing steps of the data gathered from the experiment. Section 4.1 presents the big picture of the processing steps which were conducted in the thesis project. The data processing can be divided into three steps; particle detection, three-dimensional coordinate construction, and statistical data processing. Each step is discussed in a separate section in this chapter. This chapter ends with the estimation of the uncertainty in the measurement results.

4.1. Data Processing Step

The flowchart of the experimental data processing is presented in Figure 4.1. Data processing is started from reading the file of the captured images from the experiment. Then, the process continue to crop the image to make sure only the region of interest remains on the image. After the images are cropped, the images are subtracted with the reference image which contains no particles. Therefore the remaining data in the pixels are the intensity data of the particles. Median filtering is applied to the subtracted images to reduce any distortion which can affect the particles coordinate retrieval. The particles coordinate can be acquired from the peak intensity finding process. Threshold is applied to the image in order to separate between the particles, which have high intensity, from other object. From the peak intensity finding process, the x-y and x-z coordinates of the particles are obtained. To calculate the radial and angular position of the particles, these particles coordinate have to be matched between x-y and x-z plane in order to get the three dimensional position of the particles.

As will be discussed later, there is a bias problem in the experimental results because of different particle velocity at different radial position. This bias can cause particles with slower velocity appear more frequently in the data compared to the faster particles. The bias is corrected by introducing the weighting function which is the number of frames needed for the particles to leave the field of view ($t_{r/R}$). After the bias correction, the probability distribution of the particles along the radial position $P(r/R)$ is calculated. The experimental results is studied based on this probability distribution of the particles which will be discussed later in the next chapter.

The purpose of this section is to give a big picture of the experiment data processing step. The detailed explanation of each processing step will be presented in the next sections.

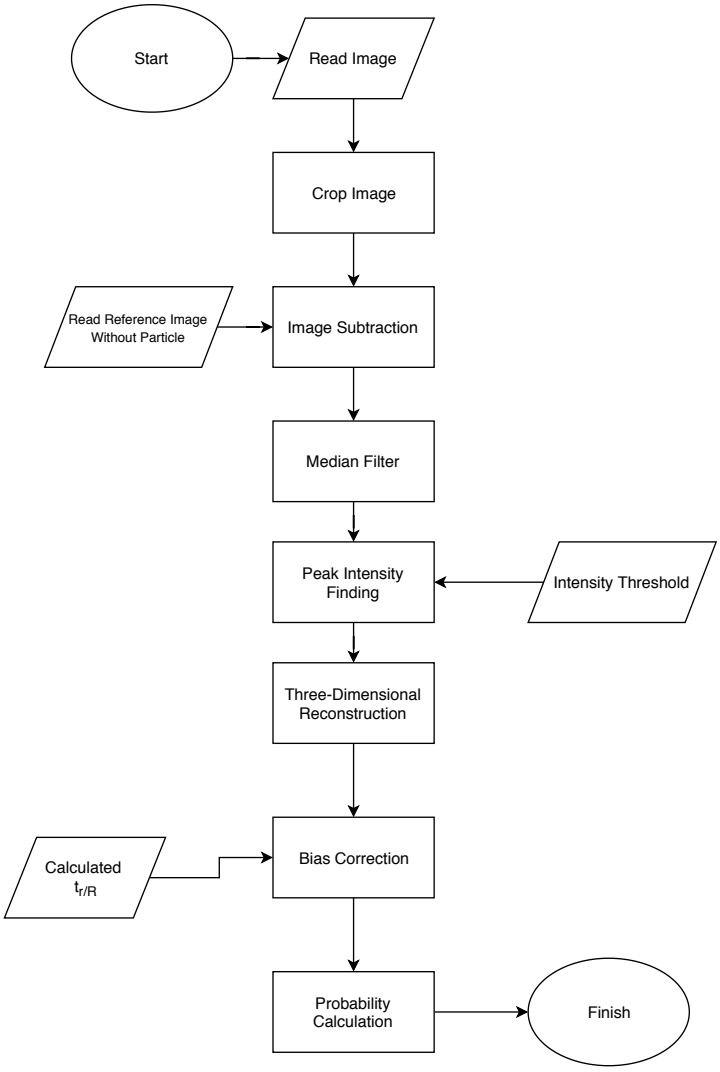

Figure 4.1: Flowchart of the experiment data processing

4.2. Particle Detection

The data processing starts with the reading of image files from the camera in Matlab. Each frame contains the image of two planes of tube, plane x-y and plane x-z. The image is cropped to remove the unnecessary part from the image in order to reduce the processing time. The cropped image of the tube is shown in Figure 4.2 (a.) and (b.).

The captured image is the arrangement of pixels which consists of the intensity level information in each pixel. The images in this thesis project were stored as an 8-bit grey-scaled value by the Davis software used. This means that the intensity level of the images ranges from 0 to 256. If a pixel has a value of 0, the pixel appears black (dark). When a pixel has a value of 256, the pixel appears white (bright). When the value closer to 0 the pixel appears darker compares to the value closer to 256.

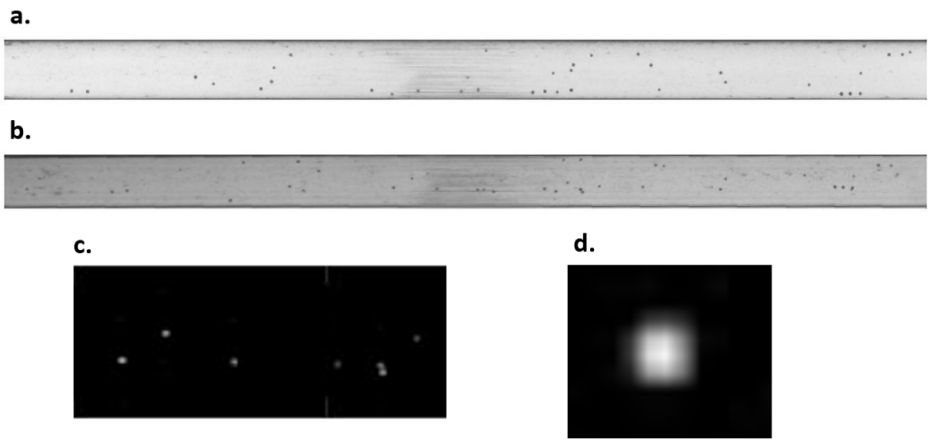

Figure 4.2: (a.) image of plane x-y and (b.) plane x-z (c.) image after background subtraction, (d.) example of a detected particle.

The next step of the image processing is the separation of the image with particles from the background. There are plenty of methods to separate the background from the image. In this project, the reference image (without the particles present) was subtracted from the captured images with moving particles. The method is illustrated in Figure 4.3. The result is an image which only contains the particles. An example of this subtracted image is shown in Figure 4.2 (c.).

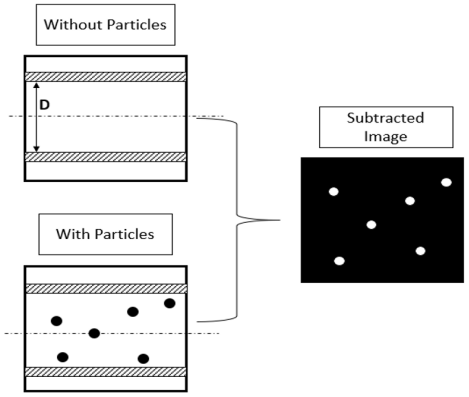

Figure 4.3: Experiment image is subtracted by the reference image which contain no particles. As a result the subtracted image will contain pixels information of particles only.

Median Filter

The processing is continued by applying median filter to the image. The purpose of using median filter is to remove noise from the image which can cause inaccuracy in the peak intensity finding. The concept of median filter is illustrated in Figure 4.4. As an example, there is an image consist of 9 pixels. Each pixel contains the intensity value which ranges from 0 to 256. Median filter works by calculating the median of the intensity value inside the evaluating window which is illustrated by the dashed box. In this example, the window has size 3x3 pixels. In the Figure, the filtering process is conducted to the pixel value located at the centre of the images, which initially has a value of 115. The intensity values inside the evaluating window are arranged from the lowest to the highest then the median can be retrieved, which is at intensity value 126. This median value (126) changes the initial intensity value of the evaluated pixel (115). The evaluating window moves to evaluate the intensity value at a

different pixel location. When a pixel is located at the boundary of images the lowest and the highest intensity value in the evaluating window will repeat itself to obtain enough entries in order to fill the 3x3 size evaluating window.

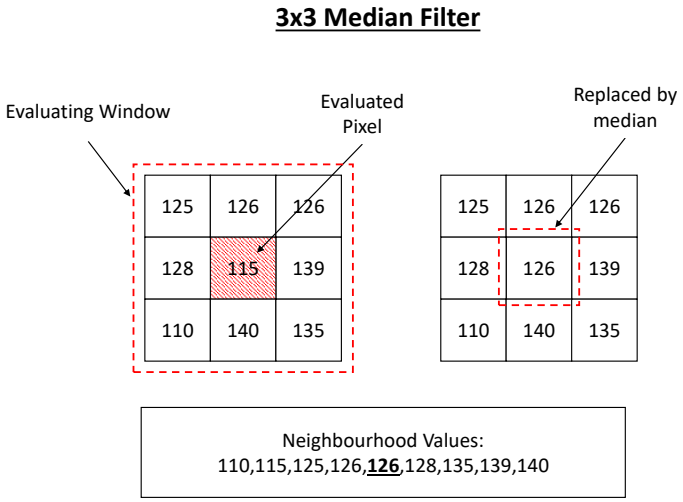

Figure 4.4: Illustration of the median filter method.

Peak Intensity Finding

After applying the median filter to the image, the peak intensity value can be obtained. If the images are properly illuminated, the location of the highest intensity is on the centroid of the sphere. The location is obtained with $pkfnd$ function in Matlab.$pkfnd$ function requires the estimated size of the particles as an input in the pixel unit. Based on particle size measurement the particle has a pixel size at about 9 pixels. This step is important to prevent the impurities in the fluid, such as small debris, to be detected as a particle. The peak intensity finding process is illustrated in Figure 4.5. The object with intensity level below the threshold will not be stored in the measurement data. It is possible that some of the particles cannot be detected due to non-uniformity in the particles illumination. Therefore, it is important to check the number of particles detected with the actual number of particles in a frame at a selected threshold.

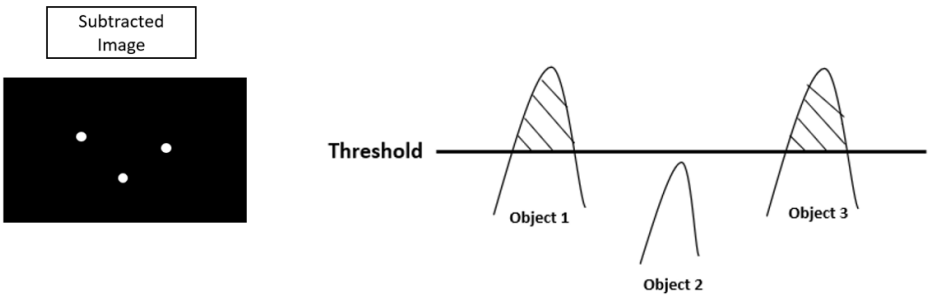

Figure 4.5: Illustration of the peak intensity finding by applying the threshold to separate between the particles and other object.

The result of the particle detection process is presented in table 4.3. The table gives the average number of particles detected in one frame for a given Reynolds number and particle concentration.

Table 4.1: The average number of particles per frame for a given Re and ϕ from the particle detection

Re	ϕ		
	0.05%	0.1 %	0.5 %
260	45	102	326
480	48	97	359
1180	46	94	339

Particle detection results are compared to the theoretical value of the number of particle at a given tube volume V_{FoV} which is calculated using following equation:

$$n_{theoretical} = \frac{V_{FoV}}{V_{particle}}\phi \tag{4.1}$$

The value of each theoretical value is compared to the average of particle detection results at a given ϕ as shown in table 4.2. It is observed that there is a difference between the theoretical and the detection results. The difference becomes more significant when the particle concentration is high, as observed in the case of $\phi = 0.5\%$. This problem occurs because with higher particle concentration the number of particles which moves above/next to each other is increasing, therefore the number of particles detected decreases.

Table 4.2: Performance of particles three-dimensional position construction in different particle-concentration

ϕ%	Theoretical particles per frame	Average particles per frame
0.05	64	47
0.1	128	97
0.5	720	341

4.3. Three Dimensional Reconstruction

Until this point, the positions of the particles in the images have been acquired. The particle position information at two plane needs to be matched to get three dimension particle coordinate from each frame, $\bar{x_j}$. The particle coordinate information in plane x-y and plane x-z shares only one similar position which is x coordinate information. By matching the x-position of a particle in both x-y and x-z plane, the 3D particle position can be obtained. This process is illustrated in Figure 4.6. The obtained 3D position will be stored in an array for each frame,$\bar{x}$.

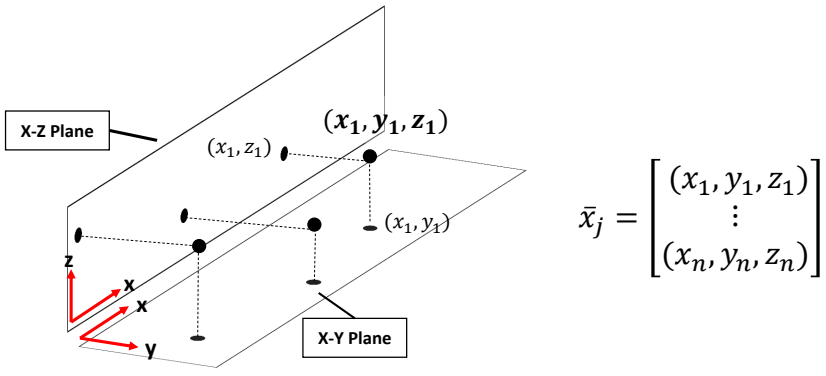

Figure 4.6: Three-Dimensional coordinate construction of the particles from information of plane x-y and plane x-z. From the information of y and z position of the particles the radial position (R_0) and angular position (θ_0) can be acquired.

In order to obtain the radial position of the particles. It is more suitable if we changes the coordinate from cartesian to cylindrical coordinate. Figure 4.7 shows the conversion process

from cartesian to cylindrical coordinate. The particles position of frame j now is stored in cylindrical coordinate in an array,$\bar{r}_j$.

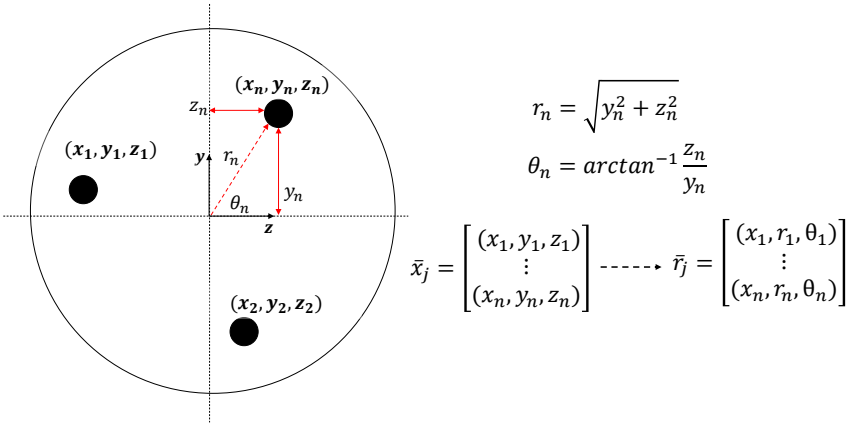

Figure 4.7: The conversion from cartesian coordinates to cylindrical coordinates. The particles position is stored in cylindrical coordinates in array $\bar{r}_j$

.

The performance of the three-dimensional particle position reconstruction is shown in Table 4.3 for different particle concentrations. The matching performance results are the average from the experiment at a given Re and L/D. The performance test also included the experiment with $\phi = 0.01\%$ to show the effect of an increase in ϕ to the percentage of particle matches.

Table 4.3: Performance of particles three-dimensional position construction in different particle-concentration

$\phi\%$	%Particles-Matched
0.01	97.0
0.05	50.1
0.1	34.3
0.5	20.3

It is shown that with an increase in ϕ the percentage of particles matched is decreasing. In the previous section, it is observed that an increase in particle concentration creates a problem in the particle detection where there are plenty of particles which moves above/next to each other. The problem is illustrated in Figure 4.8,when there is a particle which flows above/next to each other one plane only detects a particle while the other plane detects two particles at the same axial position. Therefore, there will be two candidates which are matched with one reference plane or vice versa two references for one candidate. In order to avoid the matching error, it is advisable to remove the particles with multiple candidates. The consequence is a data loss in the particle matching process. With an increase in ϕ, particles which share the same x-position in one plane are also increasing. Due to this limitation at high particle concentrations, the particle-matching method is not conducted for particles concentration above 0.5%. The study on high particles concentration in this thesis is only done by qualitative analysis of the captured images.

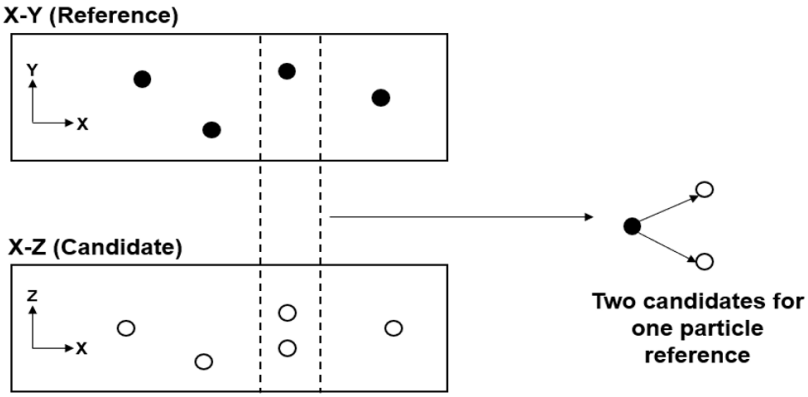

Figure 4.8: The problem at high particles concentration where one particle reference can have two candidates for its match. This is because with increase in particle concentrations the number of particles which moves next to each other is increasing. There will be missing information at one plane due to particles moving above/next to each other.

4.4. Processing and Data Statistics

4.4.1. Bias in Measurement Results

The data of the particle radial positions from three-dimensional coordinate reconstruction is constructed into histogram as can be seen in Figure 4.9 (b.).

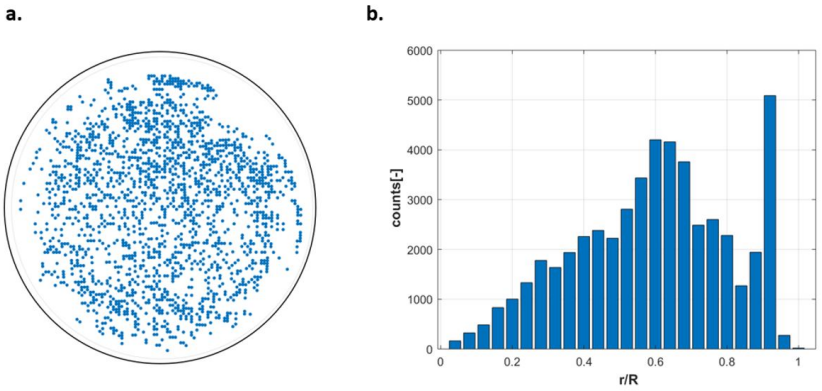

Figure 4.9: (a.) Particle radial positions at cross section of the tube and (b.) histogram of particle radial positions for $\phi = 0.05\%$, $Re = 480$, and $L/D = 250$.

The collected data from the experiment contains a bias due to the Poiseuille flow velocity profile. The problem can be explained in a simple case of particles flowing in Poiseuille flow as illustrated in Figure 4.10. Initially, ten particles were uniformly distributed across the tube cross-section at the inlet of the tube. From the shape of the Poiseuille flow velocity profile, the particles which closer to the wall move slower compared to particles move at the tube-axis. When a camera is used to capture the position of particles at a particular size of field of view and frame rate, it is possible that a particle is captured multiple times because its velocity is slower than the frame rate of the camera. Therefore, in the second frame, the particle which has been captured in the first frame still retains within the field of view.

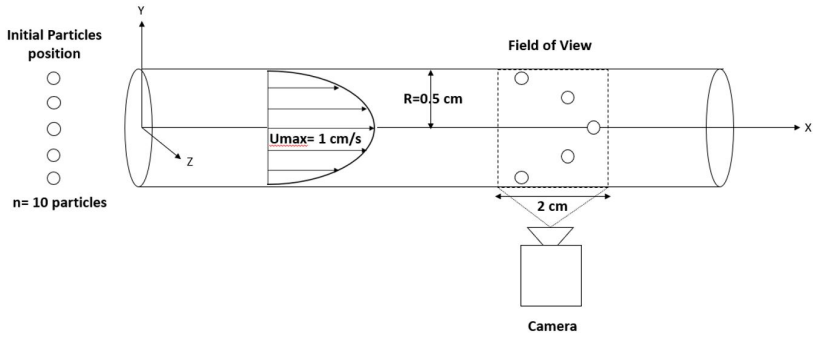

Figure 4.10: The example case of particles flowing through Poiseuille flow.

The problem is illustrated in Figure 4.11 (a.) for the example case of Poiseuille flow. The camera is taken the image at 1 frame per second for 5 seconds. Instead of 10 particles, the data will calculate 28 number of particles, as shown in the histogram of Figure 4.11 (b.). Therefore, the bias because of this velocity profile should be corrected.

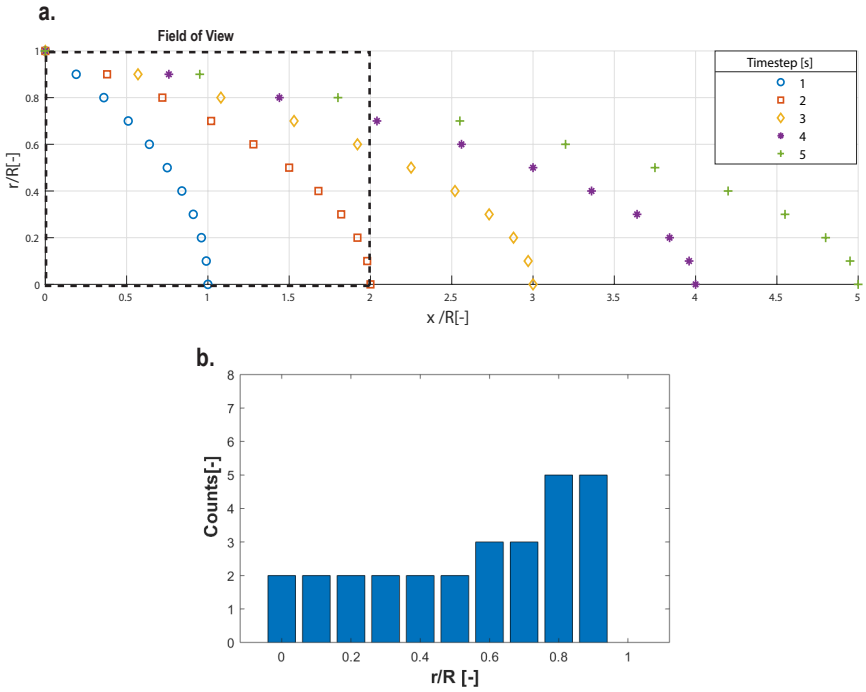

Figure 4.11: (a.) number of particles taken from the Poiseuille flow case for 5 time steps. The fastest particles (tube-axis) is passing the field of view after two time step, while for the particle closest to the wall it will appear 5 times. (b.) The number of particles captured by the camera at field of view in 5 time steps. Instead of showing 10 number of particles (which is the actual amount of particles), the camera captured 28 number of the particles for five time steps.

In order to correct this bias, the weighting function is introduced. In this case, the number of particles in the data (n) is proportional to $(t_{r/R})$ which is the number of frames needed for particles to leave the field of view. $t_{r/R}$ can be calculated using following equation:

$$t_{r/R} = \frac{l}{u(r)} f \tag{4.2}$$

where f is the frame rate, l is the length of the field of view, and $u(r)$ is the velocity of particles

at a given radial position (r).

From Figure 4.11 (b.) it can be seen that the particle close to the wall at $r/R = 0.9$ is captured five times which is more compared to the particle in the centre-line at $r/R = 0$ which is obtained for two times. The number of frames needed for particles at the center-line ($r/R = 0$) to leave the field of view is two frames ($t_{r/R} = 2$) at one frame per second, while particles near the wall ($r/R = 0.9$) leave the field of view after ten frames ($t_{r/R} = 10$).

The true number of particles (n_{true}) can be acquired when the number of particles at each radial position (n) is divided by $t_{r/R}$ which acts as the weighting function as shown in following equation:

$$n_{true} = \frac{n_{r/R}}{t_{r/R}} \tag{4.3}$$

Using equation 4.3 to correct the number of particles in the previous example of Poiseuille flow cases will yield the total amount of particles, $n_{true} = 10$, which is the actual number of particles in the example. Figure 4.12 is the comparison between the corrected number of particles to the uncorrected number of particles in the Poiseuille flow case example.

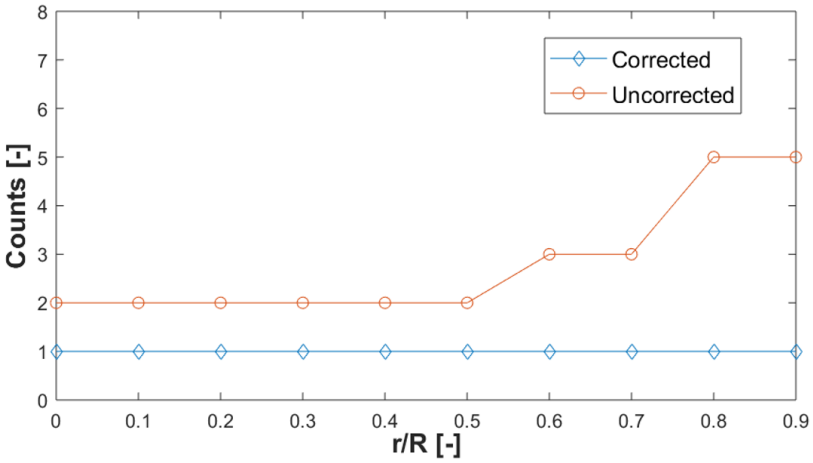

Figure 4.12: Comparison of the number of particles at each radial position of the simple Poiseuille case for corrected and uncorrected bias.

4.4.2. Bias Correction to Measurement Results

The correction method requires to calculate the axial velocity for each radial position. In a Poiseuille flow, axial velocity for any given radial position can be calculated using equation 4.4 for laminar flow [44]:

$$u(r) = u_{max}\left(1 - \frac{r^2}{R^2}\right) \tag{4.4}$$

Where u_{max} is the maximum axial velocity at the centre-line $r = 0$. There exists a relation that $u_{max} = 2U_m$ [44]from the derivation of the equation.

Before using equation 4.4, we have to make sure that the velocity profile of the experimental data is parabolic. From literature study, the presence of suspended particle in the flow can change the shape of the velocity profile [6]. This change can be either from the accumulation of the particles at the tube axis or the transition in the flow regime from laminar to turbulence regime.

Particle Tracking Velocimetry (PTV)

An investigation is done to the shape of the velocity profile using particle tracking velocimetry (PTV). The PTV method in the experiment is based on particle-pair matching which used the 'nearest neighbor' approach as illustrated in Figure 4.13. Particle images in the next frame which gives the smallest displacement to the reference particles in the reference frame is the proper particle match. The method is suitable for a very dilute suspension flow. From the experiment, it is difficult to determine the velocity profile at $\phi \geq 0.1\%$. Thus, at such condition the shape of the velocity profile is concluded from the previous studies.

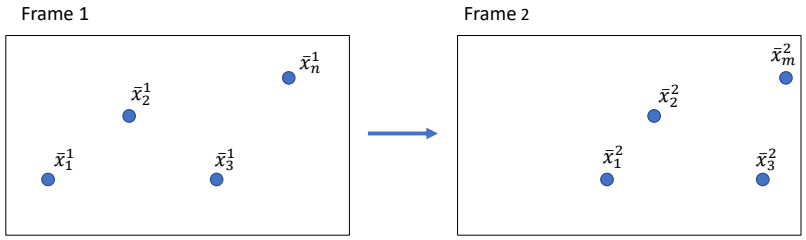

$$D_{ij} = \left|\bar{x}_i^1 - \bar{x}_j^2\right| = \begin{pmatrix} \left|\bar{x}_1^1 - \bar{x}_1^2\right| & \cdots & \left|\bar{x}_1^1 - \bar{x}_m^2\right| \\ \vdots & \ddots & \vdots \\ \left|\bar{x}_n^1 - \bar{x}_1^2\right| & \cdots & \left|\bar{x}_n^1 - \bar{x}_m^2\right| \end{pmatrix}$$

Figure 4.13: Nearest neighbor scheme is used to match particles in successive frame. D_{ij} is a deviation matrix consisted of the error between frame 1 and frame 2. The minimum error value is gained, by finding the particle in frame 2 which led to the minimum contribution in the total error between frame 1 and frame 2.

PTV results are shown in Figure 4.14 for $\phi = 0.05\%$. It is observed that there is no significant change in the shape of the velocity profile at $\phi = 0.05\%$ for each Reynolds number. Based on previous studies the shape of velocity profile of suspension will not change before $\phi = 0.14\%$ [11, 18]. Therefore, it is safe to assume that at $\phi = 0.1 - 0.5\%$ the parabolic shape of the velocity profile is unchanged. As mentioned before the change in velocity profile can also be caused by the change in the flow regime. It has been reported that the presence of the dispersed phase in the flow can change the transitional Reynolds number. The change depends on the concentration of particles and the size of the particles. Based on the previous result [20] the selected Reynolds number in this experiment is still in the laminar regime. Therefore, there is no change in the shape of the velocity profile due to change in the flow regime.

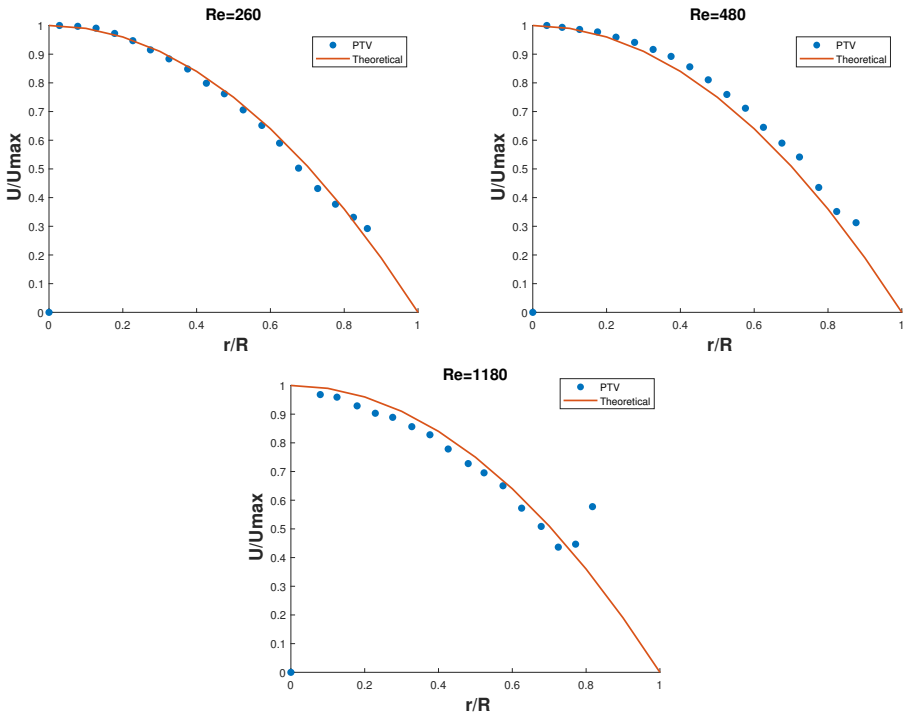

Figure 4.14: Measured velocity profile from particle tracking for particle concentration $\phi = 0.05\%$ for $Re = 260$, $Re = 480$, and $Re = 1180$.

After ensure that the flow velocity profile is parabolic. The correction method is applied to all measurements performed in the thesis project. Figure 4.15 is an example of a correction result to the measurement data. The significant effect of the correction method is a decrease in the number of particles in each histogram bin.

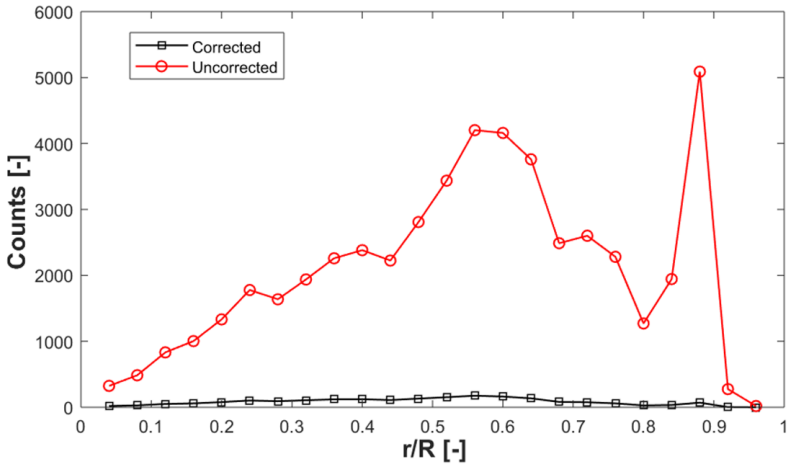

Figure 4.15: The correction method is applied to the measurement result for $\phi = 0.05\%$, $Re = 480$, and $L/D = 250$. It is shown that the number of particles at the bias corrected plot is significantly decreasing.

Based on the correction applied to each experimental results, the total number of particles in each run is varying with particles concentration. Approximately the total number of particles are 1000, 5000, and 10000 for ϕ = 0.05, 0.1, and 0.5% respectively. The number is significantly less than the total particle positions captured in 2000 frames. This condition is due to a significant decrease in the number of particles in each radial position from the bias

correction method.

4.4.3. Probability Distribution

The next step is to calculate the probability distribution of particles along the tube radial position. The data from the corrected histogram is normalized to yield the probability to find a particle in a certain radial position, $P^*(r/R)$. The general probability at a radial position r/R and angle θ is defined as $P(r/R,\theta)$. The relation between $P^*(r/R)$ and $P(r/R,\theta)$ becomes [22]:

$$P^*(r/R) = \pi^{-1}\int_0^{2\pi} P(r/R,\theta)rd\theta \tag{4.5}$$

Assuming that the probability only depends on the variation of the radial position $P(r/R,\theta)$ becomes $P(r/R)$ and can be written as equation 4.6[22]:

$$P(r/R) = \frac{P^*(r/R)}{2r} \tag{4.6}$$

Using equation 4.6, the probability distribution of the particles can be determined. This step is taking into account the error in probability due to the difference in a bin (radial) size as illustrated in Figure 4.16. The bin closer to the centre line will have less area compared to a bin closer to the wall.

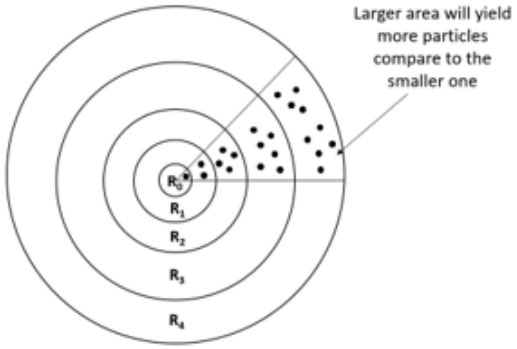

Figure 4.16: The error in probability due to differences in bin size.

The example result of the probability distribution of particles radial position is shown in Figure 4.17. Compared to the previous uncorrected histogram in Figure 4.9; the probability ($P(r/R)$) are distributed more uniform along the radial position of the tube.

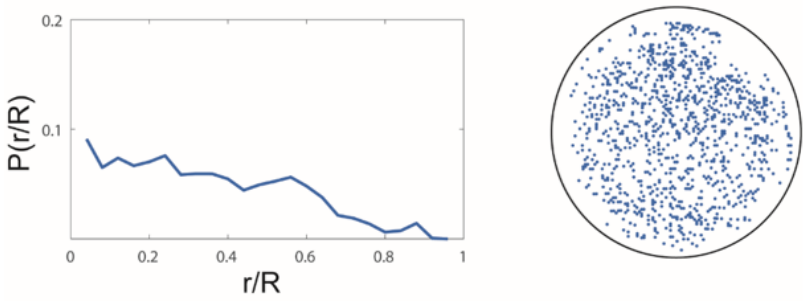

Figure 4.17: Probability distribution of particles radial position along the tube length for ϕ= 0.05%, Re= 480, and L/D= 250.

4.5. Uncertainty in Measurements

The next step is to determine the uncertainty of the probability distribution of the experimental results. The uncertainty is coming from the fact that the number of particles is limited in each bin. The uncertainty is calculated using the Bernoulli distribution approach. In this approach a random variable (N) is divided into two conditions, N=1 means particles are located inside a bin of the histogram and N=0 means that particles are located outside a bin.

Back to the probability distribution result from Figure 4.17, in this result the probability of particle located in the first bin with a range from r/R = 0 to 0.04 is $P[0, 0.04] = 0.095$. This means that there is 9.5% chance that the particle will be located at this bin, on the other hand there is 90.5% chance that the particle will be located outside this bin as illustrated in figure 4.18.

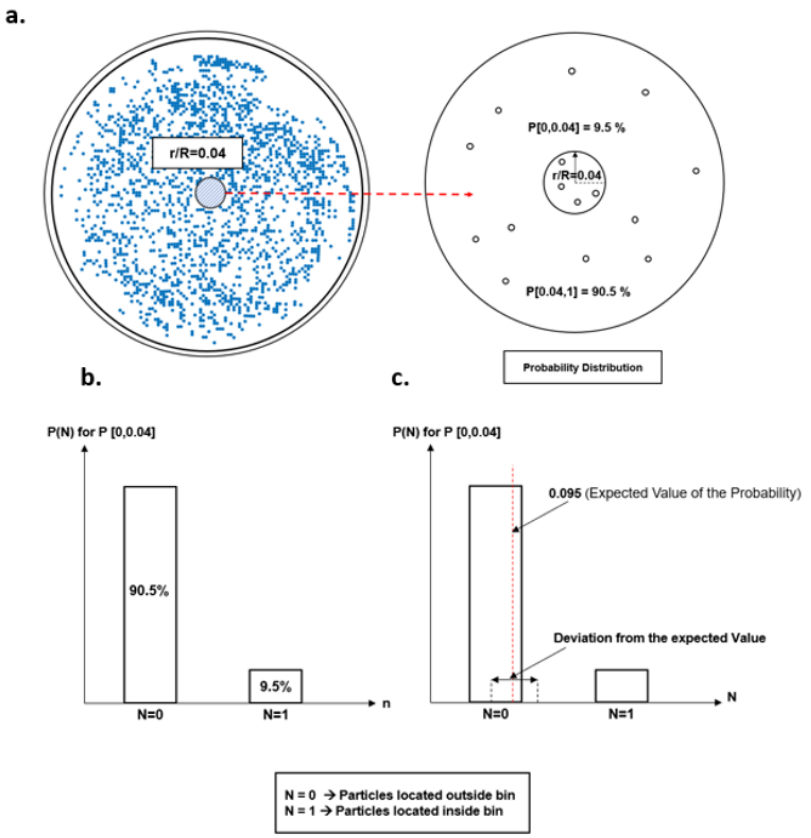

Figure 4.18: (a.) Probability distribution of particle located inside bin $r\ /\ R$ = 0-0.04 (b.) The Bernoulli distribution of the particles located in bin, r/R =0-0.04. N=0 means that the particles are located outside the bin and N=1 means that the particles are located inside the bin (c.) The expected value of the measurements $E(X)$ in the Bernoulli distribution.

The Bernoulli Distribution is shown in Figure 4.18 for the particles located inside the bin r/R = 0-0.04. The expected value of the measurement ($E(X)$) in the Bernoulli distribution is derived as follows from Peacock [29]:

$$E(X) = P(N = 1) \times 1 + P(N = 0) \times 0$$
$$E(X) = P(N = 1) \tag{4.7}$$

For this case $P(N = 1)$ is equal to 0.095, thus the expected value of the measurement $E(X) = 0.095$. The variance of the expected value ($Var[X]$) in the Bernoulli distribution can be calculated by using equation 4.8 from Peacock et al. [29]:

$$Var[X] = P(N = 1)(1 - P(N = 1)) \tag{4.8}$$

Standard deviation (σ) is the square root of the variance, and it gives the information about how the data is dispersed from the expected value X. The purpose of calculating standard deviation is to calculate the standard error ($\bar{\sigma_x}$), using equation 4.9, which determines the uncertainty of the measurements. The standard error is highly dependent on the number of particles in the measurement n, the higher this number, the smaller the error of the probability distribution.

$$\bar{\sigma_x} = \frac{\sigma}{\sqrt{n}} \tag{4.9}$$

The calculated standard error is plotted with $P(r/R)$ as shown in Figure 4.19. It can be seen that the highest uncertainty is located near the centre of the tube ($r/R < 0.04$) at $\Delta P(r/R) = \pm 0.0225$. Similar results are shown when the same step is applied into other experimental parameters. A high uncertainty at the center of the tube is due to small number of particles that are found inside the bin closed to the centre-line. Therefore, the physical phenomena closed to the centre-line should be interpreted with this uncertainty in mind. The uncertainty of the measurements can be decreased by increasing the number of frames captured. As mentioned before in Chapter 3, for every experiment 2000 frames of particle image are captured. A Higher number of frames will decrease the uncertainty of the measurement results, but this comes at the cost of storage space and increased time for data processing.

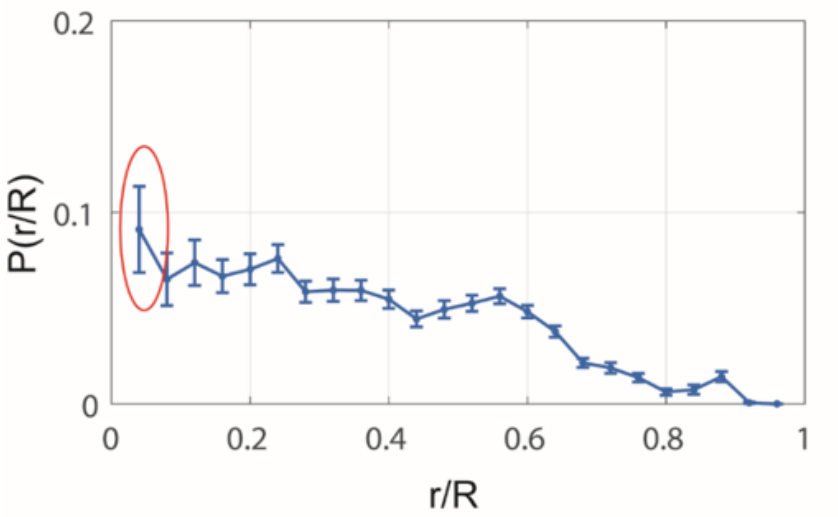

Figure 4.19: Uncertainty of the probability distribution of the radial position of the particles for ϕ = 0.05%, Re = 480, at L/D=250. The red circles is the location where the uncertainty is significantly high.

5

Results and Discussion

This chapter presents the experimental results and discussion of the physical phenomena that occur. Section 5.1 displays the results on the development of the particles along the tube length. Additionally, the effect of Reynolds number and particle concentration on the particle migration development are presented in this section. Subsequently, the observation on the secondary phenomena following the particle migration is discussed in section 5.2 for the inner annulus and section 5.3 for the trains of the particle. The chapter ends with a discussion on the results of the experiment at high particle concentration, ϕ=0.8% and ϕ=1.6% and the investigation of the buoyancy effect to the experiment results.

5.1. Development of the Particles Radial Distribution Along the Tube Length

This section presents the development of the particle radial distribution at different observation distance with respect to the tube inlet (L/D). The presentation is divided into three particle concentrations (ϕ), 0.05%,0.1% and 0.5%. For each particle concentration, the effect of Reynolds number to the development of particle distribution is presented. This section ends with the discussion of the observed combination effect between Reynolds number and the particle concentrations to the development of the particle migration.

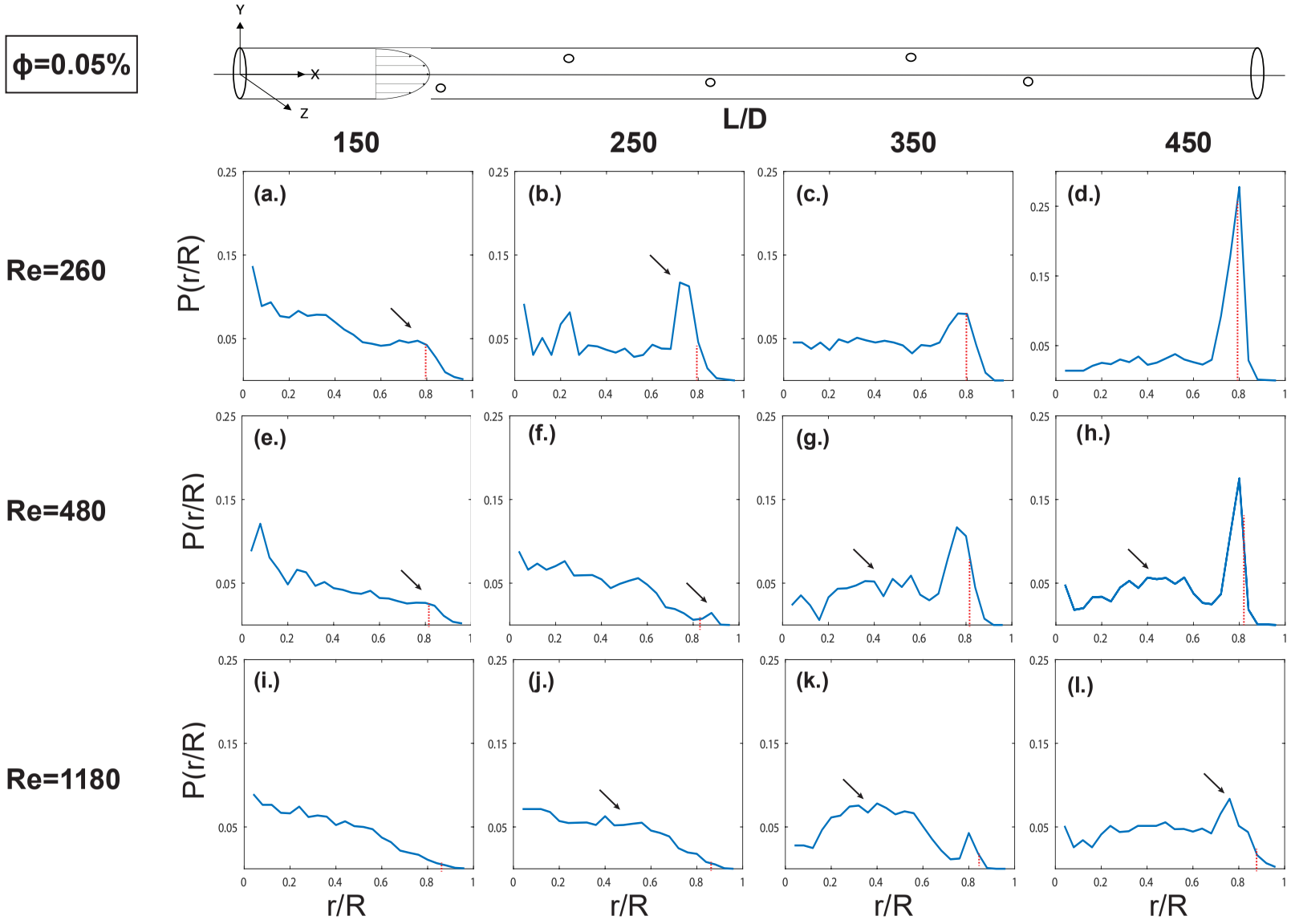

Figure 5.1: The development of particle radial distribution for $\phi = 0.05\%$. The dashed line is the expected equilibrium position based on Matas et al.[22]

5.1.1. Particle Concentration = 0.05%

The evolution of the particle radial distribution along the tube length at three different Reynolds number for $\phi = 0.05\%$ is presented in Figure 5.1. At the closest observation distance to the tube inlet ($L/D = 150$) the particles are uniformly distributed for all Re. The early process of the particle accumulation is observed for $Re = 260$ and $Re = 480$, as pointed by an arrow in Figure 5.1(a.) and (e.). For $Re = 1180$, the accumulation cannot be observed yet, as shown in Figure 5.1(i).

At the next observation distance, $L/D = 250$, the particles are distributed differently for different Re. For $Re = 260$ and 480, as already observed in the previous observation distance, the particle accumulation in the equilibrium position continues to develop. The accumulation can be observed from a narrow distribution of particles at the radial position close to the wall which is at the Segré-Silberberg equilibrium position as pointed by an arrow in Figure 5.1 (b.) and 5.1 (f.). The accumulation of particles at the equilibrium position for $Re = 260$ is higher compared to $Re = 480$. For $Re = 1180$, the particle distribution has not shown any sign of the particle accumulation. However, as pointed by an arrow in Figure 5.1(j), a movement of particles to the direction of the wall is indicated by a gradual decrease of $P(r/R)$ at the radial position close to the centre-line of the tube.

At $L/D = 350$, particle accumulation is observed for all Reynolds number as shown in Figure 5.1 (c.),(g.) and (k.). At this observation distance, the appearance of the particle accumulation becomes more apparent compared to the previous distances. It is observed from the appearance of the peak in the probability distribution at the equilibrium position ($r/R \approx 0.8$). The inner annulus is observed for $Re = 480$ and $Re = 1180$. The appearance of the inner annulus is indicated by the presence of the second peak in the probability distribution besides the peak at equilibrium position. This second peak is the sign of the appearance of the inner annulus, it is pointed by the arrow in Figure 5.1(g.) and 5.1(k.). The discussion on the presence of the inner annulus will be presented later in the next section.

At the farthest observation distance with respect to the tube inlet, $L/D = 450$, the accumulation of particles is more concentrated into a narrow region at the equilibrium position as shown in Figure 5.1(d.), (h.) and 5.1(l.). Compared to the other Reynolds number, for $Re = 1180$, the height of the peak is at the lowest. This is an indication that for $Re = 1180$ the particles are migrated at a longer distance compared to the lower Reynolds number. The same trend is also displayed from the comparison between $Re = 260$ and $Re = 480$, where at $Re = 260$ the probability of the particles at the equilibrium position is higher compared to $Re = 480$.

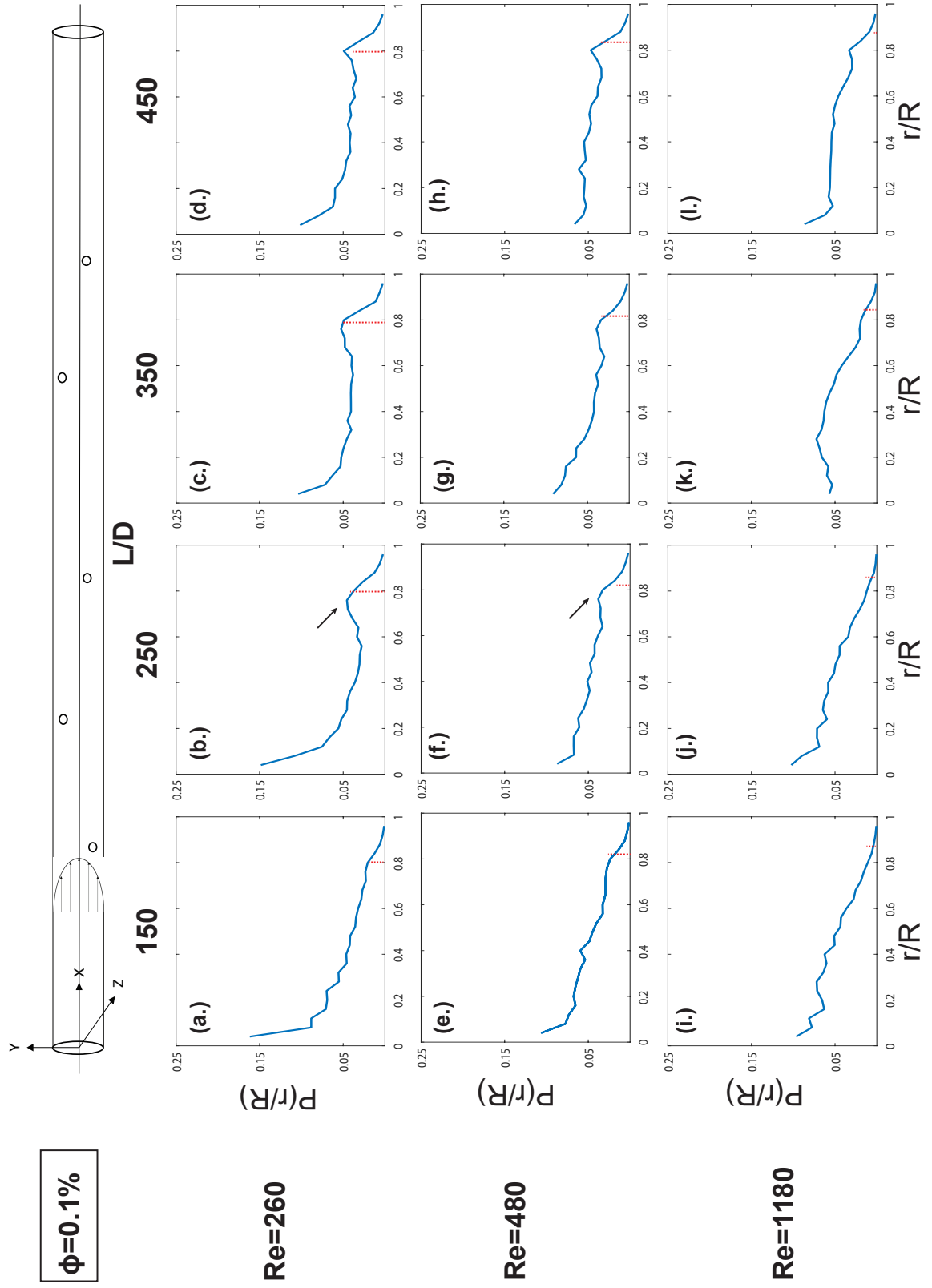

Figure 5.2: The development of particle radial distribution for $\phi = 0.1\%$. The dashed line is the expected equilibrium position based on Matas et al.[22]

5.1.2. Particle Concentration = 0.1 %

The evolution of the particle radial distribution along the tube length for $\phi = 0.1\%$ is presented in Figure 5.2. The clear effect of an increase in the particle concentration is an increase in the dispersion of the particles along the tube cross-section. At $L/D = 150$, the particle distribution is showing the same result as the $\phi = 0.05\%$, which the particles are uniformly distributed along the tube cross-section. However, there is a significant increase in the number of particles accumulated at the centre-line of the tube. Figure 5.2 (a.) shows that there is high probability $P(r/R)$ to find the particles at the centre-line of the tube. It is observed that the lower the Reynolds number the higher the probability to find the particles at the center-line of the tube.

The accumulation of the particles in the equilibrium position increases at a slower rate compared to $\phi = 0.05\%$. At $L/D = 250$, the presence of the accumulation is observed for both $Re = 260$ and $Re = 480$, as pointed by an arrow in Figure 5.2 (b.) and (f.). There is a significant decrease in the level of particle accumulation compared to $\phi = 0.05\%$ for both Reynolds number. For $Re = 1180$ there is no sign of the accumulation of particles at the equilibrium position.

At the next observation distance,$L/D = 350$, the particles are still dispersed along the tube cross-section with the development of a small peak at the equilibrium position for $Re = 260$ and $Re = 480$. Figure 5.2 (k.) shows that for Re=1180 the accumulation is not observed at this observation distance.

The accumulation of particles at the equilibrium position is observed at $L/D = 450$ for all Reynolds number. Lower Reynolds number is observed to display more apparent sign of the accumulation compared to higher Reynolds. Moreover, there is an indication that at higher particle concentration the accumulation becomes less apparent. Compared to $\phi = 0.05\%$ at the same observation distance, the probability at the equilibrium position is significantly lower compared to the other radial position.

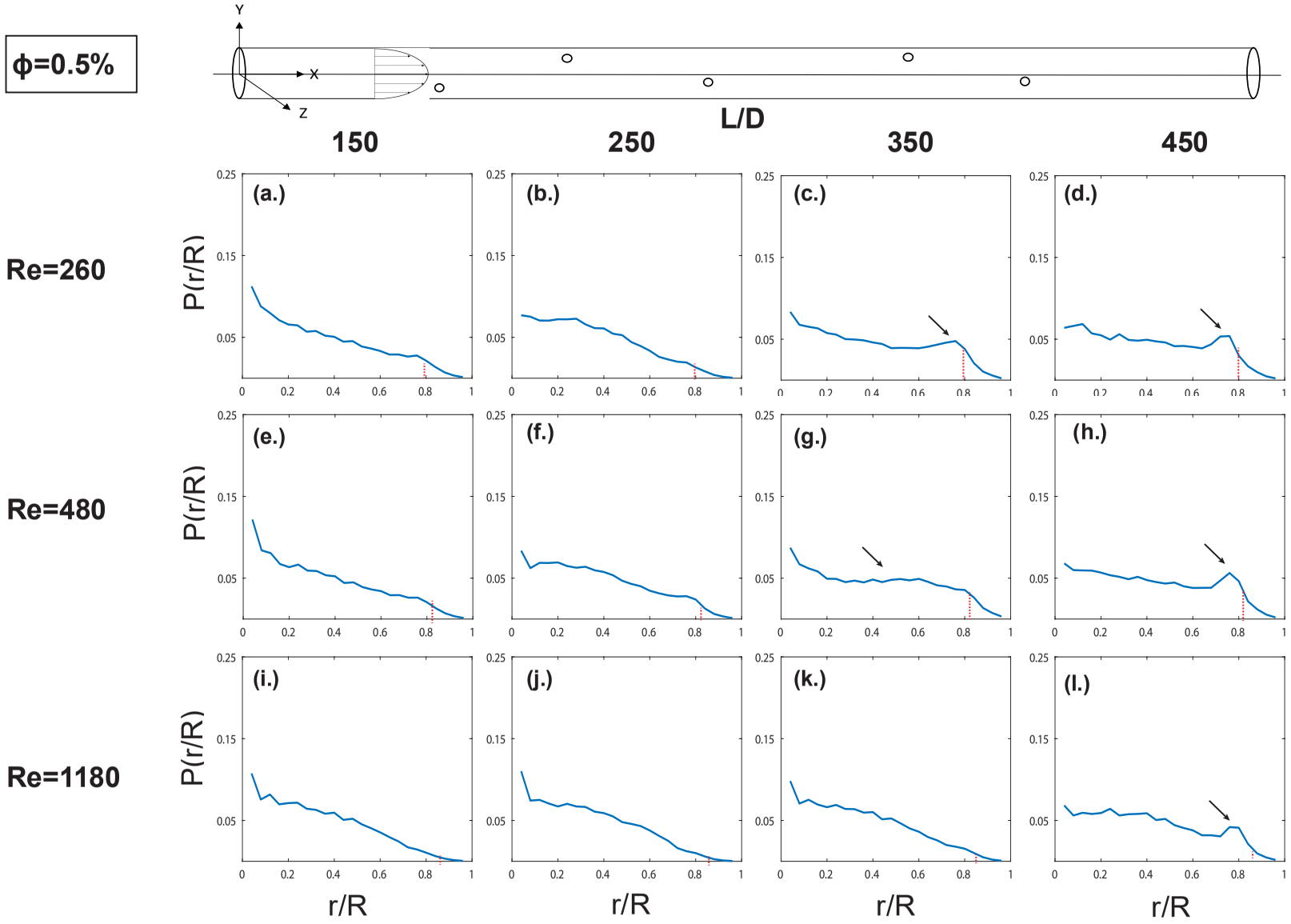

Figure 5.3: The development of particle radial distribution for $\phi = 0.5\%$. The dashed line is the expected equilibrium position based on Matas et al.[22]

5.1.3. Particle Concentration = 0.5%

From the previous section, It has been displayed that an increase in particle concentration increased the dispersion of particles along the tube cross-section. As a result the accumulation of particles at the equilibrium position becomes less apparent. The same trend is shown for $\phi = 0.5\%$, as shown in Figure 5.3. At this concentration level, the accumulation is observed at a longer distance from the inlet compared to $\phi = 0.1\%$. Even for $Re = 260$ and $Re = 480$ the accumulation is not observed before the particles reached $L/D = 450$. At $L/D = 450$. The accumulation is indicated by the appearance of a small peak for every Re as pointed by an arrow in Figure 5.3(d.),(h.) and (l.). As observed in $\phi = 0.01\%$ there is a decrease in the probability at the equilibrium position with higher particle concentration, The same result is also shown at this concentration. However, the probability difference is not that significant compared to $\phi = 0.01\%$.

For the effect of Reynolds number to the development of particle distribution interesting result is occurred, which at this concentration the accumulation starts to become more apparent at the same distance for all Re. However, there is an indication that for lower Re the accumulation process is more gradually with an increase in the distance from the inlet. The difference is most evident at $L/D = 350$, at $Re = 260$ the probability distribution has displayed a sign of the accumulation as pointed by an arrow in Figure 5.3(c.). For $Re = 480$ the sign of the accumulation is observed from a gradual decrease of probability at radial position closer to the center-line as pointed by an arrow in Figure 5.3(g.). While for $Re = 1180$ there is no apparent sign of the accumulation at the probability distribution.

5.1.4. Discussion on the Development of Particle Distribution Results

Based on the results of the development of particle distribution along the tube length, a conclusion can be derived on the effect of Reynolds number and particle concentration in altering the development of particle distribution along the tube length.

The results of the development of particle distribution along the tube length show that an increase in Reynolds number leads to a delay in the accumulation of particles at the equilibrium position. These results are consistent for all particle concentrations in this thesis study as shown in Figure 5.1, 5.2, and 5.3. This observation agrees with the results from Morita et al.[25] on the effect of Reynolds number to the development of particle migration. It is indicated that an increase in Reynolds number will lead to an increase in the migration-distance for particles to reach the equilibrium position. Figure 5.4 shows the probability to find the particles around the equilibrium position at $0.7 \leq r/R \leq 0.9$ (P_{outer}). The rate of the particle accumulation at the equilibrium position can be estimated by the linear fit of P_{outer} as a function of L/D. It is observed that the higher the Reynolds number results in a lower accumulation rate, as shown in Figure 5.4(a.) for $\phi = 0.05\%$.

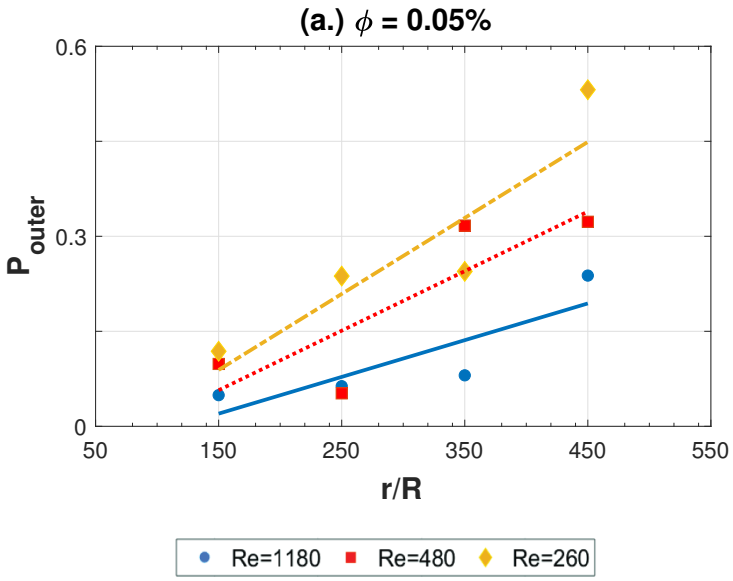

Figure 5.4: (a.) Probability to find the particles at radial position $0.7 \leq r/R \leq 0.9$ (P_{outer}) as a function of the observation distance for $\phi = 0.05\%$. The linear fit gives the expected rate of particles accumulation at the equilibrium position. It follows that with an increase in Reynolds number, the rate become slower.

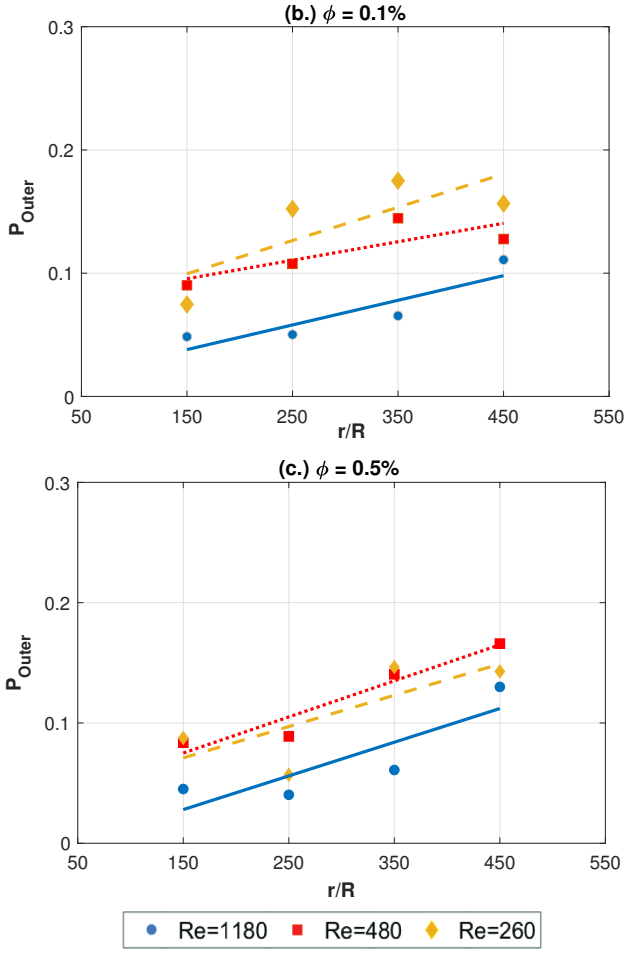

(b.) and (c.) Probability to find the particles at radial position $0.7 \leq r/R \leq 0.9$ (P_{outer}) as a function of the observation distance for $\phi = 0.1\%$ and 0.5%. the rate of the accumulation is slowing as the particle concentration increase. It follows that the effect of Reynolds number to the accumulation rate is less significant at higher ϕ .

The rate of the particle accumulation is also estimated for $\phi = 0.1\%$ and $\phi = 0.5\%$ as shown in Figure 5.4 (b.) and (c.). It is observed that an increase in ϕ leads to a lower rate of particle accumulation. There is an indication that the effect of Reynolds number on migration-distance becomes less significant at higher particle concentration. From the observation on the rate of accumulation for $\phi = 0.5\%$, there is no significant difference in the accumulation rate for different Reynolds number.

The higher the concentration the sign of the accumulation at the equilibrium position becomes less apparent. This condition is shown in Figure 5.4 that P_{outer} at farthest observation distance from the inlet is significantly lower for $\phi = 0.1 - 0.5\%$ compared to $\phi = 0.05\%$. This result corresponds to an increase in the dispersion of the particle along the tube radial position as particle concentration increases. The slowing down of particle accumulation rate with an increase in particle concentration can also be directed to an increase in dispersion. An increase in the particle dispersion induces the particle-particle interaction at the radial position between the centre-line and the wall of the tube [11]. This particle-particle interaction opposes the inertial effect which directed the particles to move in the direction to the wall. The resistance corresponds to the hydrodynamic interaction between the particles in the form wake generated by the spherical particles [28]. This generated wake resist the migration of the particle to the equilibrium position.

The Observation of the equilibrium position results is shown in Figure 5.5. The equilibrium position is selected as the radial position between $0.7 \leq r/R \leq 0.9$ where the maximum probability $P(r/R)$ lies. The Figure also presents the previous results of the equilibrium position from Matas et al. [22] and Sègre-Silberberg [38]. The experiment results show a slight discrepancy from Matas et al equilibrium position results which can be directed to the difference in the particle size used in the experiment. However, with an increase in particle concentration, it is observed that the difference in the equilibrium becomes slightly higher. This increase corresponds to the movement of the equilibrium position closer to the center-line as the particle concentration increases.

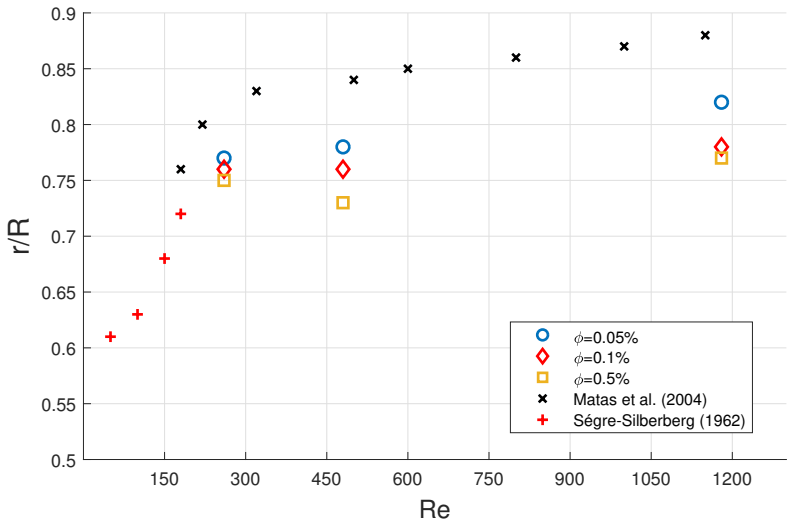

Figure 5.5: The equilibrium position as a function of the Reynolds number. It is shown that for this thesis experiment result the equilibrium position is located closer to the center-line compare to the previous results from Matas et al. [22]. There is an indication with an increase in particle concentration the equilibrium position will move closer to the center-line

5.2. Inner Annulus Appearance

As mentioned in section 5.1, the inner annulus is observed in this thesis results at $\phi = 0.05\%$ for $Re = 480$ and $Re = 1180$. The appearance of the inner annulus is indicated by the appearance of the second peak which is located close to the centre-line as shown in Figure 5.6. In the same Figure, the Polar-scattered plot of the detected radial positions of the particles is presented to observe the presence of the two annuli on the tube cross-section. As observed from the scatter plot, the Sègre-Silberberg annulus has a narrower distribution compared to the inner annulus.

Figure 5.1 shows that the inner annulus is vanishing with a further distance from the inlet. This result agrees with Morita et al.[25] which observed that there is only Segré-Silberberg annulus presents at the fully-developed condition of particle migration. This result supports the conclusion that the inner annulus is just a transient phenomenon in the process of the particles migrate to the Segre-Silberberg equilibrium position.

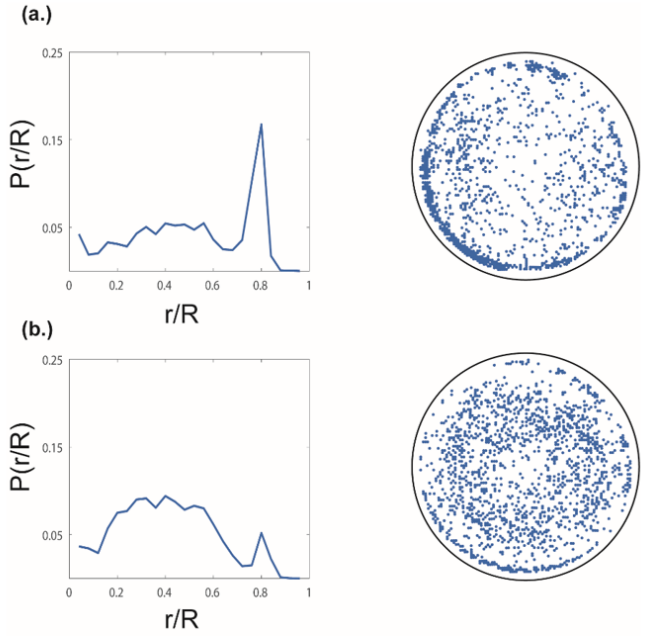

Figure 5.6: The appearance of the inner annulus in the experiment results at particles concentration 0.05% for Re=480 and (b.) Re=1180.

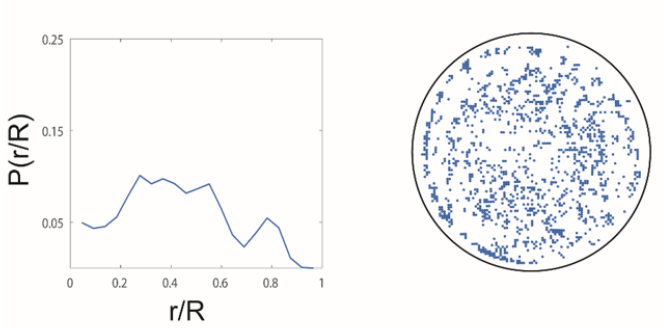

Figure 5.7: The appearance of the inner annulus in the experiment results at particles concentration 0.01% for Re=1180.

Particle concentration is observed to be an important factor in affecting the appearance of the inner annulus. In the case of $\phi < 0.05\%$, Figure 5.7 shows the appearance of the inner

annulus at $\phi = 0.01\%$ for $Re = 1180$. For $\phi > 0.05\%$, there is no appearance of the inner annulus in every observation distance. This result can be related to the increase in the dispersion of the particles as the particle concentration increases. At higher particle concentration the particle will be more distributed throughout the cross-section of the tube. This condition is more difficult for the formation of the inner annulus. Furthermore, experimental result indicates that there is a limitation in the particle concentration for the inner annulus appearance. This condition can be explained from computational simulation results from Shao et al.[39], which stated that an increase in particle concentration will resist the formation of the inner annulus.

5.3. Trains of Particles

In this thesis experiment, the trains of particles are observed as shown in Figure 5.8. This thesis only study the observation on the formation of the particle trains for $\phi = 0.05\%$ and $\phi = 0.1\%$. From the experiment at $\phi = 0.01\%$, there was no trains formation observed. The absence of trains formation because of high separation distance between particles at low particle concentration. Thus, the interaction between particles is unlikely to present. For $\phi > 0.1\%$, there was a difficulty in distinguishing the train structure from the rest of the particles, due to a high number of particles existed in a frame.

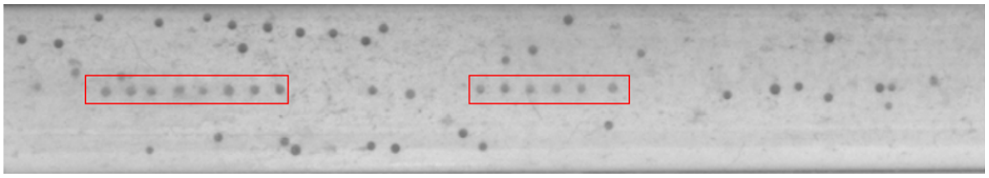

Figure 5.8: The Trains of particles observed from the conducted experiment (red-box)

Radial Position of the Trains

The measurement is conducted on the position of the observed trains at different observation distance (L/D). The Train radial position was determined with a similar approach as the three-dimensional coordinate construction which was explained in chapter 4. The result is shown in Figure 5.9 for ϕ=0.05%, which the position of the trains are observed to be located around the equilibrium position at $r/R \approx 0.8$. For $Re = 1180$, the trains are not found before $L/D = 350$. This is because the formation of trains is closely related to the accumulation of particles at the equilibrium position [21]. Figure 5.1 shows that the accumulation of particles for $Re = 1180$ is started to appear at $L/D = 350$, which is the same distance where the trains are started to appear. Figure 5.9 presents that there is no significant difference in the trains radial position for different Reynolds number.

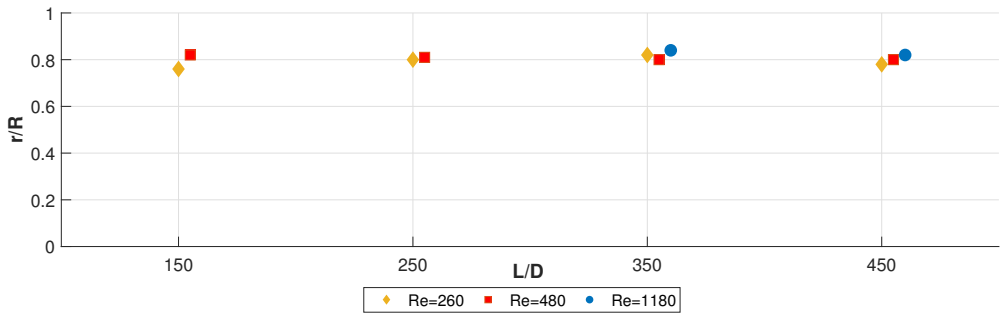

Figure 5.9: Average position of the trains at different observation distance (L/D) for particles concentration $\phi = 0.05\%$ as a function of Re. It follows that the location of the trains is at the equilibrium position.

The Effect of Reynolds Number

The effect of the Reynolds number and the particle concentration are studied by calculating the number of trains formed at the variation of these parameters. Figure 5.10 shows the development of particle trains formation with a further distance from the inlet at $Re = 260, 480,$ and 1180. The percentage of particles in the trains is the ratio between the particles which are located in trains over the total number of particles. An increase in the number of particles in trains is observed with an increase in L/D. The cause of the increase is suggested to be related to the development of particle migration. It is observed that the accumulation of the particles at the equilibrium position is increasing with an increase in L/D. The increase in the number of particles at the equilibrium position can lead to an increase in the probability of the particles to form a train.

Figure 5.10 also shows the effect of Reynolds number on the formation of trains. It is shown that the formation of particle trains is the highest at $Re = 480$. This result is contradictory with the argument that the formation of the trains is due to the accumulation of particles at the equilibrium position. From Figure 5.1 it is observed that the highest accumulation is observed at $Re = 260$. This result shows that the percentage of particles in the trains are the highest in $Re = 480$ not in $Re = 260$ where the accumulation is observed to be higher. It is because the factor which is altering the trains formation is not only the number of the particles in the equilibrium position but also the hydrodynamic interaction between the particles [14]. The same result is also reported by Matas et al.[21] in Figure 2.6 which shows that the amount of the particles in the train is increasing with the Reynolds number until it reached the peak at $Re \approx 600$ then it starts to decrease. Matas et al. analysed this results through the mechanism of the particle trains formation. It is reported that the particles formed a train due to the particle trapped in the reversed flow which generated around the particles when particles Reynolds number $Re_P >> 1$, as illustrated in figure 2.14. The size of the reverse flow area will increase with an increase in Re_P, that is the reason when the Re increases there will be more trains formed. The reason for a decrease in the formation of trains after $Re \approx 600$ is related to a decrease in the accumulation of particle at the same L/D for a higher Re. Thus, the effect of an increase in the size of the reverse flow region with a higher Re is surpassed by the deficiency in the number of particles at the equilibrium position.

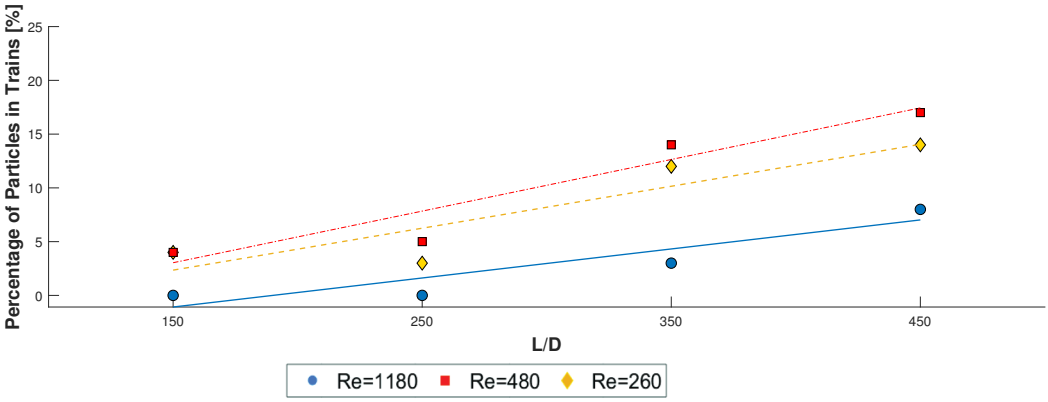

Figure 5.10: The percentage of the particles in the trains as a function of observation distance (L/D) for $\phi = 0.05\%$. The number of the particles in trains is the most for $Re = 480$ at every observation distance.

The Effect of Particle Concentration

Figure 5.11 shows that with the higher ϕ the number of the particle in trains is increasing, except for the case of $Re = 1180$. The effect of the particle concentration on the formation of the trains is explained with the existence of a distance preferred between particles (Δs). Humphry et al [14] postulated that at sufficiently low ϕ only a single train is formed when the number of particles per unit length in the x-direction (λ) is increasing until $1/\lambda = \Delta s$, another train is formed. Δs itself is observed to depend on the Reynolds number, as observed

by Matas et al.[21], Δs is decreased with an increase in Re_p. With a higher ϕ the distance between particles (δ) will decrease, this condition will ease the formation of the trains of the particles.

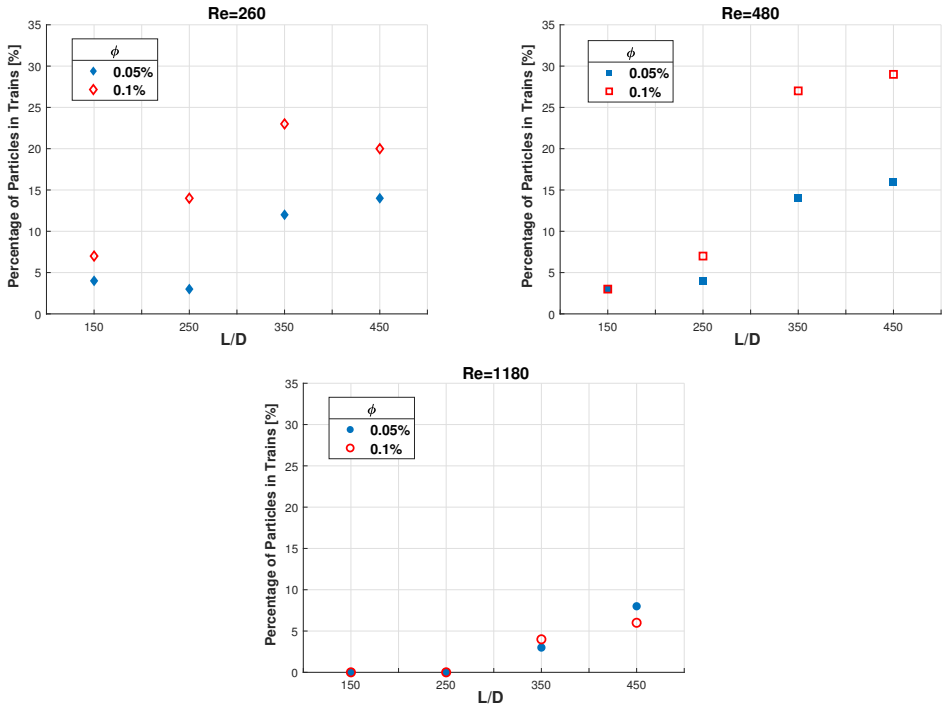

Figure 5.11: Comparison of the percentage of the particles in trains along the observation distance (L/D) at $\phi = 0.1\%$ and $\phi = 0.05\%$ for $Re = 260, 480$, and 1180. An increase in the percentage of particles in the trains is observed as the particle concentration increases, except for $Re = 1180$.

However, there is a discrepancy for the result at $Re = 1180$, the number of particle in the trains is decreasing instead of increasing for a higher ϕ. In section 5.1, particle accumulation is observed to be delayed into the longer distance to the tube inlet with an increase in ϕ. Although it is not the case for $Re = 260$ and $Re = 480$, at $Re = 1180$ the delay in the accumulation causes a decrease in the formation of trains. It is suggested that this discrepancy is due to a combination effect between the deficiency of the particles concentrated at the equilibrium position and a decrease in the preferred distance between particles (Δs) in the trains as Reynolds number increases. Even though the distance between particles is decreasing with higher particle concentration, it cannot accommodate the mentioned combination effect for the particles to form more trains compare to lower Reynolds number.

5.4. Results of The Experiment at High Particles Concentration.

The experiment method in this thesis project has a limitation in analyzing the case of particle concentration higher than 0.5%. Therefore, the discussion on $\phi > 0.5\%$ is only conducted with a qualitative analysis from the picture of the particles in the tube. Figure 5.12 and 5.13 are the pictures of the x-y plane of the tube for $\phi = 0.8\%$ and $\phi = 1.6\%$ for three different Re at $L/D = 450$. The longest observation distance is selected to see the development of the particle at the farthest location with respect to the tube inlet. From the observation in section 5.1 with a higher ϕ, the particles will be migrated into a longer distance with respect to the tube inlet. Because of the limitation in the experimental setup, the observation cannot move longer than $L/D = 450$.

The particle distribution shows that the particle dispersion along the tube cross section

is increasing with the Reynolds number, as shown in Figure 5.12. For Re =260, the accumulation of the particle at the top and bottom side of the tube are observed, as pointed by the arrow in the same figure. As Reynolds number increases the accumulation is decreasing, and the distribution is found to be more uniform through the tube cross-section. An increase in the particle concentration to $\phi = 1.6\%$ causes an increase in the accumulation of particles at the top and bottom side of the tube. The accumulation also appears not only for Re =260 but also for $Re = 480$ as pointed by an arrow in Figure 5.13. While for $Re = 1180$, there is no sign of accumulation of particles at the top and bottom side of the tube. These results can be an indication of the presence of the buoyancy effect in the experiment results.

The effect of non-neutrally buoyant fluid to the migration is studied theoretically by Vasseur and Cox [43] and Hogg [13]. It was reported that the presence of a slight buoyancy effect to the migration will bring heavier particles to the bottom of the tube and lighter particles to the top side of the tube. The slight buoyancy effect to the particle distribution is also discussed in Matas et al.[22] report. It is reported that even for a slight dispersion in the fluid density for about $\Delta\rho = \pm 0.003 kg/m^3$, the light and heavy particles tend to migrate to the equilibrium positions closer to the top and bottom of the tube. While for the neutrally buoyant particles will be distributed along the equilibrium position. The buoyancy number describes the effect of the buoyancy, $B = U_m/u_s$ [13], where u_s is the settling velocity. B explains the ratio between the inertial effect to the buoyancy effect, a low value of B means that the buoyancy effect more dominant compared to the inertial effect and vice versa.

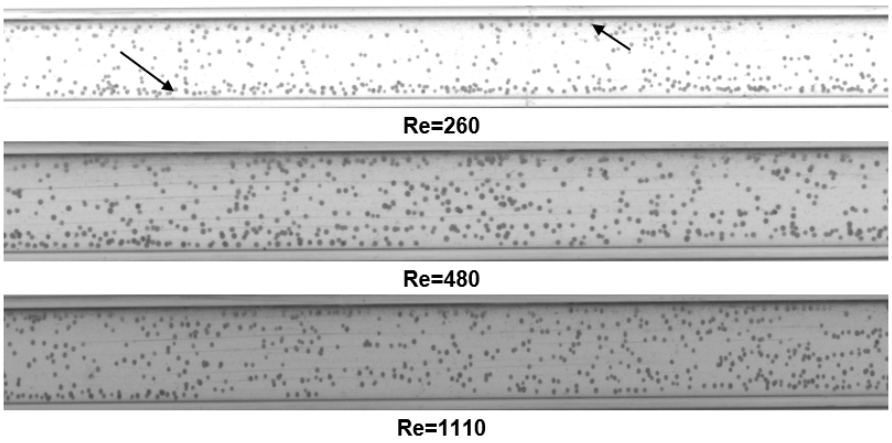

Figure 5.12: Pictures of x-y plane of the tube which show the particles distribution for $\phi = 0.8\%$ at observation distance $L/D = 450$ for Re=260,480,1110. The lower the Reynolds number, it is indicated that the particles tend to accumulate at the top and bottom side of the tube as pointed by the arrow. The accumulation is due to a slight dispersion in fluid density to the neutrally-buoyant condition which causes the heavy and light particles migrate to the equilibrium position at the top and bottom of the tube.

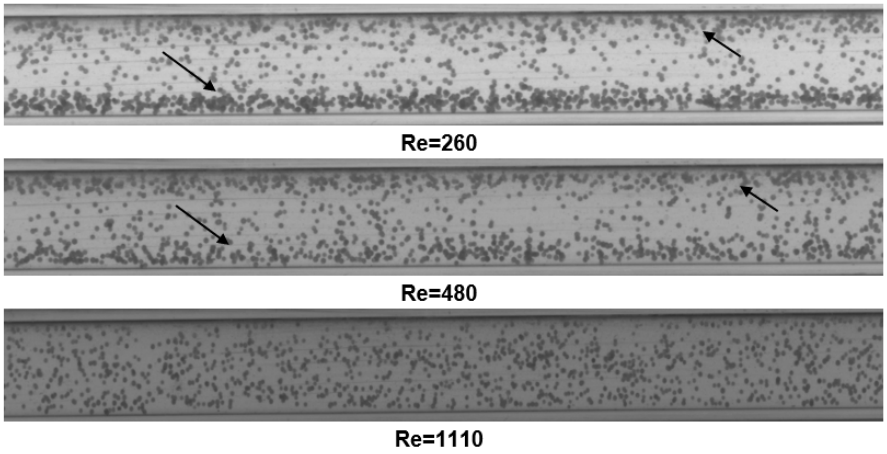

Figure 5.13: Pictures of x-y plane of the tube which show the particles distribution for ϕ =1.6% at observation distance $L/D = 450$ for $Re = 260, 480, 1110$. The arrow pointed to the increase in the accumulation of particles at the top and bottom side of the tube with an increase in particle concentration. It follows that the accumulation also appears for $Re = 480$. This is because an increase in the buoyancy effect with an increase in particle concentrations.

The observation of Matas et al. regarding the buoyancy effect can explain the top-bottom accumulation occurrence for $\phi = 0.8\%$ and $\phi = 1.6\%$. As seen in Figure 5.12 the accumulation of the particles at the top and bottom side of the tube only appears at $Re = 260$, which is the smallest Reynolds number in the experiment. A lower Reynolds number means that the inertial effect will be less dominant than the buoyancy effect. An increase in the particle concentration, as observed in Figure 5.13, will increase the number of the particles distributed at the top and bottom side of the tube. This condition is caused by an increase in the buoyancy effect due to an increase in particle concentration. Mcnown and Lin [24], Bogardi [3], Cheng [5] reported the settling velocity (u_s) is increasing with particle concentration. It means that the B value becomes lower for the same Re. Because of this increase, the buoyancy effect becomes more dominant than the inertial effect. As a result, the accumulation at the top and bottom of particles appeared for $Re = 480$. While for $Re = 1180$, there is no top-bottom accumulation to be found. It is because at this Reynolds number the inertial effect more dominant compared to the buoyancy effect.

The analysis on the high particle concentration brings an important attention to study the migration for high particle concentration at the neutrally buoyant environment. The buoyancy effect which is initially not dominant at the low ϕ can become more significant as ϕ increase. Even for a slight difference to the neutral buoyant condition this effect can become significant at high ϕ.

5.5. Investigation of the Buoyancy Effect in the Experiment Results.

In order to investigate the buoyancy effect on the experiment results, the radial position distribution of the particles is plotted for each parameter from the experiment results in section 5.1. The tube cross-section is divided into six bins as illustrated in Figure 5.14. Then, the fraction of the number of particles detected at each bin to the total particles detected is plotted ($n*$), as shown in Figure 5.15. The sign of the presence of the buoyancy effect can be observed if most of the particles are located at one particular bin, either at the bottom of the tube (bin=1) or the top of the tube (bin=6). If the particles are distributed into a concave shape distribution, which the particles are abundant in the top and bottom of the tube then gradually decrease in the center. Then, there is a slight buoyancy effect on the experiment.

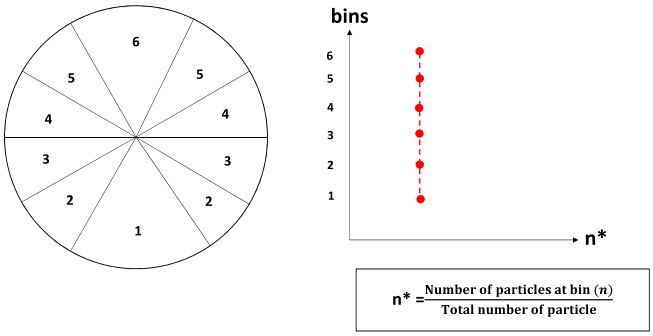

Figure 5.14: Illustration of the distribution particle radial position plotting process. The radial position of the particles are distributed into 6 bins then the ratio of the number of the particles at each bin to total particles detected (n*) is plotted as a function of each bin.

The results of the particle distribution are shown in Figure 5.15. The figure shows a vertical concave shape distribution for experiment at $\phi \geq 0.1\%$ at Re=260 and 480. The concave distribution becomes steeper as the particle concentration increases. This condition is because the buoyancy effect becomes more significant with an increase in particle concentrations. Thus, there is an increase in the number of particles at the top and bottom side of the tube as the particle concentration increases. For Re = 1180, the distribution has a shape closer to the straight line which shows that it is distributed more uniformly at higher Reynolds number. As mentioned in the previous section the buoyancy effect is less affected at a higher Reynolds due to inertial effect more dominant.

The presence of small buoyancy effect has to be a consideration in interpreting some of the physics occurring in this thesis results, especially for Re =260 and 480 at $\phi \geq 0.1\%$. For example, this effect can be a major cause of the decrease in the significance of the Reynolds number in altering the rate of the accumulation at high particle concentration as observed in section 5.1. As seen in Figure 5.15 for ϕ=0.5 % for Re = 260 and 480 the distribution showed that there is a slightly buoyancy effect in the experiment. The decrease can be directed to an increase in the buoyancy effect as the particle concentration increases instead of the hydrodynamic interaction between particle as previously concluded. For the development of particle distribution along the tube length results, it is plausible that there is an additional effect to the particle accumulation because of the particle settling at the top and bottom of the tube. Furthermore, from Matas et al. [22] it is implied that in a slightly non-buoyant fluid, the particle distribution will be closer to the center-line of the tube. This condition agrees with the equilibrium position results where this experiment has an equilibrium position closer to the center-line compared to the previous reports.

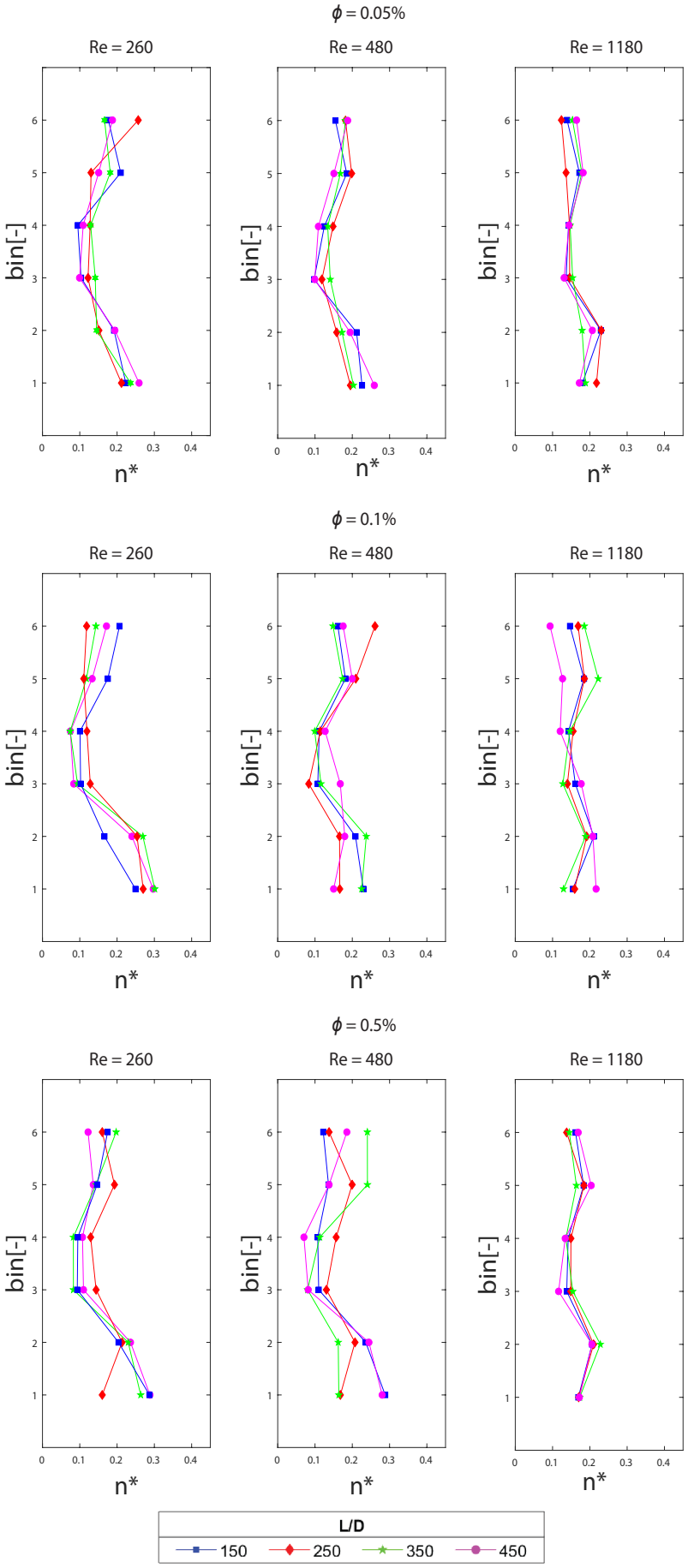

Figure 5.15: The distribution of the particles radial position at each bin for the given experiment parameters. The concave shape of the particle distribution shows the presence of slight buoyancy effect in the experimental results.

6

Conclusion and Recommendation

6.1. Conclusion

The aim of the thesis project is to study the effect of Reynolds number and particle concentration in the development of particle migration. Following the study of particle migration, the effect of the parameters to the secondary phenomena, the inner annulus and the trains of particles are also studied in this thesis project. The study was conducted using particle tracking method to capture particle radial positions at different parameters and observation distances. Based on the captured particle radial positions, the probability distribution was determined for different experimental parameters.

For the effect of Reynolds number to the development of particles migration, it is observed that an increase in Reynolds number increases the migration-distance of the particle migration. Based on the particle distribution results, for $Re = 1180$ the accumulation of the particles does not appear until $L/D = 350$, while for lower Re the accumulation process is observed started from $L/D = 250$. This result is an indication that the migration-distance is increasing with an increase in Re. The rate of the accumulation was estimated using a linear fit from the calculated probability to find the particles close to the Segré-Silberberg equilibrium position. It was observed that the accumulation rate became lower as the Reynolds number increases.

From the observation of the particle radial distribution at three different particle concentrations $\phi = 0.05\%$, 0.1%, and 0.5%, it is observed that an increase in particle concentration increases the particle migration-distance. This increase is observed from the decrease in the rate of accumulation of particles at the equilibrium position as ϕ goes higher. Furthermore, it is observed that the effect of Reynolds number becomes less significant at higher particle concentration. It indicates from the similarities in the rate of the accumulation for different Reynolds number as the particle concentration increases.

From the study of the appearance of the inner annulus, it is observed that the inner annulus vanishes with an increase in distance from the inlet. This result agrees with Morita et al.[25] which stated that the inner annulus is only a transient phenomenon rather than an equilibrium one. In the experiment result, the inner annulus is not found for the case of $\phi > 0.05\%$. This disappearance of the inner annulus corresponds to the increase in particles dispersion with higher ϕ. Therefore, it is difficult to observe the appearance of the inner annulus structure in higher particle concentration.

The study of the trains of particles shows that the formation of the train is highly related to the accumulation of particles at the Segrè-Silberberg equilibrium position. This conclusion is derived from the measurement of trains radial position, which mostly is found near the Segré-Silberberg equilibrium position. The number of trains formed is increasing with

an increase in the distance from tube inlet. This result can be related to the result of particle migration development, where the particle accumulation is increasing with an increase in distance from the inlet. Furthermore, the trains formation is also altered by the variation in particle concentration; it is observed that the trains formation increases with an increase in particle concentration. A different result is observed for the experiment at $Re = 1180$ where the number of trains formed is decreased with an increase in particle concentration. This anomaly can be related to a decrease in the preferred distance between particles in a train with an increase in Re.

6.2. Recommendation

In this section, several recommendations for the future study in a related topic of research will be suggested. The recommendation will be divided into two parts, recommendation to the experimental technique and recommendation for future study.

6.2.1. Recommendation on Experimental Technique

In order to study the particle migration, this thesis relies on the optical technique to detect the particle radial positions. There is a huge data loss due to the size of the field of view in the experiment. As previously discussed in chapter 4, the technique which is used in this thesis produces a bias due to a high number of frames needed (t) for the particles to leave the field of view. As a consequence, the same particles recorded multiple times in the frame. A technique is proposed to correct this bias by dividing the experimental data by the number of frames needed for particles to leave the field of view of the camera. This correction method causes substantial data loss, for example, 20000 radial positions of the particles are detected from only 300 particles. Therefore, in order to decrease the data loss from using this correction method, there are two recommendations in the experimental technique:

Field of View of Camera Adjustment

The bias is present due to the shape of the velocity profile of the Poiseuille flow. By decreasing the size of the field of view, the amount of data loss from the bias correction method will decrease, as illustrated in Figure 6.1 Field of view (FOV) 1 is more extensive than FOV 2, as a consequence, a particle is captured in both frame 1 and frame 2. In the case of FOV 2, the particles have already left the field of view in frame 2. Therefore, the number of the same particles exist in multiple frames can be decreased.

However, there is a limitation in decreasing the size of the field of view of the camera. The

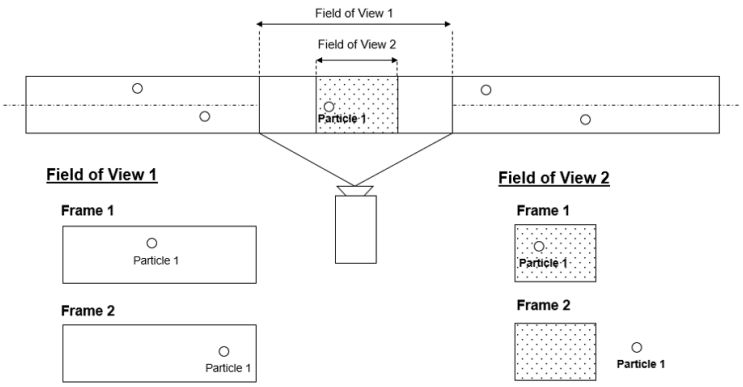

Figure 6.1: Decrease the size of field of view to decrease the amount of data loss during the experiment.

size of the field of view has to ensure the capability to capture the image of particles in each radial position. When the small field of view is selected, there is a possibility that the particles with the highest velocity, which are particles located at the centre-line ($r/R = 0$), has a travel

distance longer than the length of the field of view. So, it is suggested that the minimum size of the field of view is the travel distance of the particles located in the centre of the tube at a given frame rate. To be noted that using this solution is not completely diminish the data loss. Because the limitation of the size of the field of view is the travel distance of particle at the centre of the tube, particles closer to the wall will still appear in multiple frames.

Frame Rate Adjustment

The frame rate of the camera can be set to match with the travelling time of particles leaving the field of view. Therefore, the number of the same particles captured in multiple frames can be decreased. The frame rate is set to the rate of the particles closer to the centreline leave the field of view. If the rate is selected to be the same as the rate of the particles closer to the wall leave the field of view, then there is a high probability that the faster particles will be failed to be captured in the frame as illustrated in Figure 6.2. With this method, there is no need to decrease the size of the field of view.

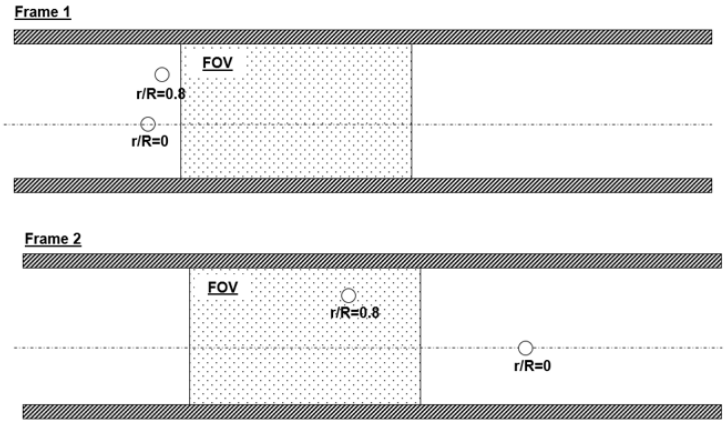

Figure 6.2: The problem when frame rate adjusted to the travel distance of the particles closer to the wall ($r/R = 0.8$) than the particles closer to the centreline.

Experiment in Multiple Observation Distance Simultaneously

In this thesis experiment, the observation at each distance was conducted at a separate run for the same experimental parameters due to the limitation in the available equipment. This method will cause slight discrepancy on the experiment results due to the change in the environmental condition during the experiment. An example of the change in the environmental condition is the change in the working fluid density due to evaporation of water. This change in density, even for a very slight change, can cause the emergence of the buoyancy effect as seen in this thesis result. If the experiment is conducted simultaneously at each observation distance, the evolution of particle radial distribution can be observed without the discrepancy in the experiment condition in mind. Therefore, the results will be more reliable, and the repeatability of the experiment will increase.

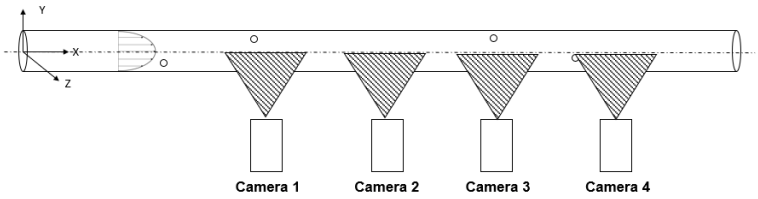

Figure 6.3: The problem when frame rate adjusted to the travel distance of the particles closer to the wall $(r/R = 0.8)$ than the particles closer to the centreline.

6.2.2. Recommendation for Future Study

Based on the study of the particle migration under Poiseuille flow, there are several recommendations for future study to enhance the understanding of the phenomena. Firstly, is the investigation to the flow field around the particles to study the hydrodynamic interaction between the particles. It has been concluded that the effect of particle concentration in delaying the particle migration is due to the hydrodynamic interaction between the particles. However, there hasn't been good documentation of the flow field around the particles to support this conclusion. Thus, an exact answer on the dynamic of the particles at reasonably high concentration cannot be derived yet. Secondly, a study on the particle distribution in the turbulence regime can be an exciting continuation of this thesis study. There will be a new challenge in studying the particle distribution in the turbulence regime especially in the selection of the experimental technique. It is still open to the possibility that new phenomena can occur following the particle migration in turbulence regime. Lastly, is the study to the individual particle trajectory to the effect of the variation of the experimental parameter. Based on the captured trajectory, the lift forces acted on the particle can be calculated at each position. The knowledge of the acted lift force can validate the previous theoretical and computational results regarding the mechanism of the migration.

Bibliography

[1] Evgeny S. Asmolov. The inertial lift on a spherical particle in a plane Poiseuille flow at large channel Reynolds number. *Journal of Fluid Mechanics*, 381:10, 1999.

[2] GK Batchelor. *An introduction to fluid dynamics*. Cambridge university press, 1967.

[3] János Bogárdi. Sediment transport in alluvial streams. Technical report, Akademiai Kiado Budapest, 1974.

[4] F P Bretherton. The motion of rigid particles i n a shear flow at low Reynolds number. *Journal of Fluid Mechanics*, (1956):284–304, 1962.

[5] Nian-Sheng Cheng. Simplified settling velocity formula for sediment particle. *Journal of hydraulic engineering*, 123(2):149–152, 1997.

[6] R. G. Cox and H Brenners. The lateral migration of solid particles in Poiskille flow- I Theory. 23(Part 2):147–173, 1968.

[7] R Fahraeus and T Lindqvist. The viscosity of the blood in narrow capillary tubes. *American Journal of Physiology*, 96(3):562–568, 1931.

[8] J. Feng, H. H. Hu, and D. D. Joseph. Direct Simulation of Initial Value Problems for the Motion of Solid Bodies in a Newtonian Fluid Part1. Sedimentation. *Journal of Fluid Mechanics*, 261:95–134, 1994.

[9] HL Goldsmith and SG Mason. The flow of suspensions through tubes. i. single spheres, rods, and discs. *Journal of Colloid Science*, 17(5):448–476, 1962.

[10] R. E. Hampton, A. A. Mammoli, A. L. Graham, N. Tetlow, and S. A. Altobelli. Migration of particles undergoing pressure-driven flow in a circular conduit. *Journal of Rheology*, 41(3):621–640, 1997.

[11] Minsoo Han, Chongyoup Kim, Minchul Kim, and Soonchil Lee. Particle migration in tube flow of suspensions. *Journal of Rheology*, 43(5):1157, 1999.

[12] B.P.; Leal Ho L.G. Inertial migration of rigid spheres in two-dimensional unidirectional flows. *Journal of Fluid Mechanics*, 65(2):365–400, 1974.

[13] Andrew J. Hogg. The inertial migration of non-neutrally buoyant spherical particles in two-dimensional shear flows. *Journal of Fluid Mechanics*, 272:285–318, 1994.

[14] Katherine J Humphry, Pandurang M Kulkarni, David A Weitz, Jeffrey F Morris, Howard A Stone, Katherine J Humphry, Pandurang M Kulkarni, David A Weitz, and Jeffrey F Morris. Axial and lateral particle ordering in finite Reynolds number channel flows Axial and lateral particle ordering in finite Reynolds number channel flows. 081703(2010):1–5, 2014.

[15] R Co Jeffrey and JRA Pearson. Particle motion in laminar vertical tube flow. *Journal of Fluid Mechanics*, 22(4):721–735, 1965.

[16] Saul Kaplun and PA Lagerstrom. Asymptotic expansions of navier-stokes solutions for small reynolds numbers. *Journal of Mathematics and Mechanics*, pages 585–593, 1957.

[17] A. Karnis and S. G. Mason. The flow of suspensions through tubes VI. Meniscus effects. *Journal of Colloid And Interface Science*, 23(1):120–133, 1967.

[18] L.G. Koh, C.J., Hookham, P., Leal. Suspension Flows in a Rectangular Channel. 266: 1–32, 1994.

[19] D. Leighton and Andreas Acrivos. The shear induced migration of particles in concentrated suspensions. *J. Fluid Mechanics*, 181(181):415, 1987.

[20] J. P. Matas, J. F. Morris, and Guazzelli. Transition to Turbulence in Particulate Pipe Flow. *Physical Review Letters*, 90(1):4, 2003.

[21] Jean Philippe Matas, Virginie Glezer, Élisabeth Guazzelli, and Jeffrey F. Morris. Trains of particles in finite-Reynolds-number pipe flow. *Physics of Fluids*, 16(11):4192–4195, 2004. doi: 10.1063/1.1791460.

[22] Jean Philippe Matas, Jeffrey F. Morris, and Élisabeth Guazzelli. Inertial migration of rigid spherical particles in Poiseuille flow. *Journal of Fluid Mechanics*, 2004. ISSN 00221120. doi: 10.1017/S0022112004000254.

[23] Martin R Maxey and James J Riley. Equation of motion for a small rigid sphere in a nonuniform flow. 883(1983), 1983.

[24] John Stephenson McNown and Pin-Nam Lin. *Sediment concentration and fall velocity*. State University of Iowa, 1952.

[25] Yusuke Morita, Tomoaki Itano, and Masako Sugihara-Seki. Equilibrium radial positions of neutrally buoyant spherical particles over the circular cross-section in Poiseuille flow. *Journal of Fluid Mechanics*, 2017.

[26] Oliver. © 1962 Nature Publishing Group. *Nature*, 196:952–953, 1962.

[27] N. Otsu. A Threshold Selection Method from Gray-Level Histogram . *IEEE TRANSACTIONS ON SYSTEMS, MAN, AND CYBERNETICS*, 9(1):855–860, 1979.

[28] Arman Pazouki and Dan Negrut. A numerical study of the effect of particle properties on the radial distribution of suspensions in pipe flow. *Computers and Fluids*, 108:1–12, 2015.

[29] Brian Peacock, John Wiley, and M Evans. *Statistical Distribution*. Wiley Interscience, 1993.

[30] C Poelma. *Experiments in particle laden turbulence, Simultaneous particle: Fluid Measurements in Grid Generated Turbulence Using Particle Image Velocimetry*. 2004.

[31] Ian Proudman and JRA Pearson. Expansions at small reynolds numbers for the flow past a sphere and a circular cylinder. *Journal of Fluid Mechanics*, 2(3):237–262, 1957.

[32] Markus Raffel, Christian E Willert, Steve T Wereley, and Jürgen Kompenhans. *Particle Image Velocimetry : a practical guide*.

[33] RV Repetti and EF Leonard. Segré-silberberg annulus formation: a possible explanation. *Nature*, 203(4952):1346, 1964.

[34] S. I. Rubinow and Joseph B. Keller. The transverse force on a spinning sphere moving in a viscous fluid. *Journal of Fluid Mechanics*, 11(3):447–459, 1961.

[35] P. G. Saffman. On the motion of small spheroidal particles in a viscous liquid. *Journal of Fluid Mechanics*, 1(5):540–553, 1956.

[36] P. G. Saffman. The lift on a small sphere in a shear flow. *Journal of Fluid Mechanics*, 22:385–400, 1965.

[37] J Schonberg and E J Hinch. Inertial migration of a sphere in Poiseuille flow. *Journal of Fluid Mechanics*, 203(June):517–524, 1989.

[38] G. Segré and A. Silberberg. Behaviour of macroscopic rigid spheres in Poiseuille flow Part 2. Experimental results and interpretation. *Journal of Fluid Mechanics*, 14(1962), 1962.

[39] Xueming Shao, Zhaosheng Yu, and Bo Sun. Inertial migration of spherical particles in circular Poiseuille flow at moderately high Reynolds numbers. *Physics of Fluids*, 20(10), 2008.

[40] M Tachibana. On the behaviour of a sphere in the laminar tube flows. *Journal of Rheology*, 12:58–69, 1973.

[41] Hans Tollert. Die wirkung der magnus-kraft in laminaren strömungen. i. teil. der quertrieb in sedimentierenden teilchenschüttungen. *Chemie Ingenieur Technik*, 26(3):141–150, 1954.

[42] Erik van Duin, Ruud Henkes, and Gijs Ooms. Influence of oil viscosity on oil-water core-annular flow through a horizontal pipe. 2018.

[43] P Vasseur and RG Cox. The lateral migration of a spherical particle in two-dimensional shear flows. *Journal of Fluid Mechanics*, 78(2):385–413, 1976.

[44] Frank M. White. Fluid Mechanics. 2016.

[45] HK Yuen, J. Princen, J. Illingworth, and J. Kittler. Comparative study of Hough Transform methods for circle finding. *Image and Vision Computing*, 8(1):71–77, 1990.